NOMA-Based Hybrid Satellite-UAV-Terrestrial Networks for 6G Maritime Coverage

Xinran Fang, *Student Member, IEEE*, Wei Feng, *Senior Member, IEEE*, Yanmin Wang, Yunfei Chen, *Senior Member, IEEE*, Ning Ge, *Member, IEEE*, Zhiguo Ding, *Fellow, IEEE*, and Hongbo Zhu

***Abstract*— Current fifth-generation (5G) networks do not cover maritime areas, causing difficulties in developing maritime Internet of Things (IoT). To tackle this problem, we establish a nearshore network by collaboratively using on-shore terrestrial base stations (TBSs) and tethered unmanned aerial vehicles (UAVs). These TBSs and UAVs form virtual clusters in a user-centric manner. Within each virtual cluster, non-orthogonal multiple access (NOMA) is adopted for agilely including various maritime IoT devices, which are sparsely distributed over the vast ocean. The nearshore network also shares the spectrum with marine satellites. In such a NOMA-based hybrid satellite-UAV-terrestrial network, interference among different network segments, different clusters, and different users occurs. We thereby formulate a joint power allocation problem to maximize the sum rate of the network. Different from existing studies, we use large-scale channel state information (CSI) only for optimization to reduce system overhead. The large-scale CSI is obtained by using the position information of maritime IoT devices. The problem is non-convex with intractable non-linear constraints. We tackle these difficulties by adopting max-min optimization, the auxiliary function method, and the successive convex approximation technique. An iterative power allocation algorithm is accordingly proposed, which is shown to be effective for coverage enhancement by simulations. This shows the potential of NOMA-based hybrid satellite-UAV-terrestrial networks for maritime on-demand coverage.**

***Index Terms*— Hybrid satellite-UAV-terrestrial network, interference, maritime Internet of Things, non-orthogonal multiple access (NOMA), power allocation.**

Manuscript received 27 January 2022; revised 10 May 2022; accepted 4 July 2022. Date of publication 25 July 2022; date of current version 9 January 2023. This work was supported in part by the National Key Research and Development Program of China under Grant 2020YFA0711301; in part by the National Natural Science Foundation of China under Grant 61941104 and Grant 61922049; in part by the King Abdullah University of Science and Technology Research Funding (KRF) under Award ORA-2021-CRG10-4696; and in part by the Tsinghua University–China Mobile Communications Group Company Ltd., Joint Institute. The associate editor coordinating the review of this article and approving it for publication was M. Sheng. *(Corresponding author: Wei Feng.)*

Xinran Fang, Wei Feng, and Ning Ge are with the Beijing National Research Center for Information Science and Technology, Department of Electronic Engineering, Tsinghua University, Beijing 100084, China (e-mail: fxr20@mails.tsinghua.edu.cn; fengwei@tsinghua.edu.cn; gening@tsinghua.edu.cn).

Yanmin Wang is with the School of Information Engineering, Minzu University of China, Beijing 100041, China (e-mail: yanmin-226@163.com).

Yunfei Chen is with the School of Engineering, University of Warwick, Coventry CV4 7AL, U.K. (e-mail: yunfei.chen@warwick.ac.uk).

Zhiguo Ding is with the School of Electrical and Electronic Engineering, The University of Manchester, Manchester M13 9PL, U.K. (e-mail: zhiguo.ding@manchester.ac.uk).

Hongbo Zhu is with the Coordination Innovative Center of IoT Technology and Application (Jiangsu), Nanjing University of Posts and Telecommunications, Nanjing 210003, China (e-mail: zhuhb@njupt.edu.cn).

Color versions of one or more figures in this article are available at https://doi.org/10.1109/TWC.2022.3191719.

Digital Object Identifier 10.1109/TWC.2022.3191719

I. Introduction

NOWADAYS, the fast development of maritime economies fosters the maritime Internet of Things (IoT). They not only require ubiquitous connectivity but also put high demands on latency and reliability [1], [2]. Building a comprehensive maritime communication network has been recognized as a consensus globally. Although advanced fifth-generation (5G) techniques bring much convenience to ground networks, they still cannot support efficient coverage on the sea. At present, the maritime communication system mainly consists of two parts: terrestrial base stations (TBSs) and marine satellites. TBSs have limited coverage, while satellites usually have low data rates and large transmission delays, which make the communication on the sea far from satisfying. How to construct an effective maritime network remains open.

Generally, satellites are recognized as an indispensable part of global coverage. We have witnessed a rapid development of satellite communication in recent decades [3], [4]. But it is still more efficient to rely on advanced terrestrial techniques for nearshore areas [5]. It is reported that most maritime communication demands occur within the exclusive economic zone [6]. In this sense, a wide-band nearshore network is expected. However, TBSs are mostly deployed on high lands to overcome the influence of the earth's curvature, where basic infrastructures such as optical fibers are hard to deploy. This leads to site scarcity problems of TBSs, and relaying them only becomes increasingly insufficient. To address these issues, unmanned aerial vehicles (UAVs) can join in as communication facilities [7]. Their easy-deployment merits could help alleviate the site problem of TBSs. Due to the generally higher altitude, UAVs can also provide wider coverage and better channels [8], [9]. Moreover, their on-demand dispatch working mode inherently supports content coverage, which is suitable for maritime IoTs that need to download or upload certain contents within a given time [10]. Promisingly, these aerial nodes could further be equipped with computing modules to support the coverage enhancement [11]. In a word, the coordination of TBSs and UAVs deserves to be well designed, so as to extend the efficient terrestrial services farther from the shore.

In addition, to accommodate the wide sparsity of maritime IoT [12] and agilely serve different users, the non-orthogonal multiple access (NOMA) transmission scheme can be considered [13], [14]. This scheme is designed to serve a group of users within one resource block; thus, more connections and higher spectrum efficiency can be achieved compared with the orthogonal multiple access (OMA) [15], [16]. In addition, NOMA can implement the successive interference cancellation (SIC) to extract far users' interference from near users' signals [17]. Far users can be better attended without much compromise of the system efficiency.

Considering aggravated spectrum scarcity problems, nearshore networks may share the spectrum with marine satellites. With the aid of NOMA, we believe such a NOMA-based hybrid satellite-UAV-terrestrial network is promising to bring new opportunities on the sea [7]. Nevertheless, it also faces unique challenges. Due to the geographical limitation of both deploying TBSs and dispatching tethered UAVs, the nearshore network is irregular, leading to complicated co-channel interference. In addition, the nearshore network and the satellite have mutual interference. In this study, we address these problems, to show the potential gain of NOMA-based hybrid satellite-UAV-terrestrial networks for maritime coverage enhancement. In particular, we exploit the unique features of maritime communication channels and maritime users and accordingly design a joint resource allocation scheme to maximize the sum rate of the nearshore network with practical constraints, including affordable system overheads and low computational complexity.

A. Related Works

To the best of our knowledge, few studies have explored the potential of UAVs on the sea. To improve the rate of a maritime user, Li *et al.* [18] leveraged a fixed-wing UAV and jointly optimized the UAV's trajectory and power. Fang *et al.* [19] and Wang *et al.* [20] extended the scenario to a multi-UAV case and optimized the system sum rate and the minimal user rate, respectively. Zhang *et al.* [21] utilized the UAV as a relay and optimized its placement, so as to extend the nearshore coverage. In addition, with only TBSs and satellites, Wei *et al.* [5] utilized maritime environment information to estimate channel states, which were further utilized to instruct the precoding design. Xiao *et al.* [22] devised a voyage-based cooperative resource allocation scheme, so as to reduce system power consumption. These studies provide valuable references for the improvement of hybrid maritime networks. But none of them takes the wide sparsity of maritime IoT into account, and the corresponding coverage scheme is still missing.

NOMA provides a promising solution to cover widely and sparsely distributed IoT. To exploit its efficiency, the inter-user interference should be well addressed. In the literature, power allocation has been widely applied to tackle different interference. In [23], Ali *et al.* investigated both uplink and downlink NOMA for the case of a single antenna. The authors maximized the sum rate of all users by optimizing both user pairing and the power allocation. Sun *et al.* [24] jointly considered the power allocation and subcarrier allocation policy for a NOMA full-duplex system to maximize the weighted throughput. Wu *et al.* [25] did a solid work for a relay-assisted downlink network, where NOMA is applied for both BS-relay and relay-user links. A power allocation scheme was proposed to maximize the throughput, which achieves a significant improvement of OMA. Zhang *et al.* [26] proposed a novel idea to let the near user to act as a full-duplex relay for the far user. The authors analyzed the NOMA performance in terms of the outage probability and the ergodic sum rate. The optimal power allocation factor was also derived in closed form. Moving a further step, multi-antenna NOMA was investigated in [16], [17], [27]–[29]. Sun *et al.* [16] considered the sum-rate maximization for a multi-input multi-output (MIMO) NOMA system. The optimal power allocation scheme under a specific channel state information (CSI) condition and a sub-optimal scheme applicable to all cases were derived. Furthermore, the authors proposed both optimal and low-complexity sub-optimal power allocation schemes to maximize the ergodic capacity with only statistical CSI [27]. Ding *et al.* [17] investigated the precoding and detection matrix design for MIMO NOMA. The impacts of user scheduling and power allocation were also evaluated to show the superiority of NOMA over OMA. To further consider inter-cluster interference, Ali *et al.* [28] developed linear beamforming to cancel the inter-cluster interference and devised a dynamic power allocation scheme to maximize the overall capacity. Sun *et al.* [29] jointly optimized beamforming and power for a novel setting where users are clustered by their requirements rather than the effective channel order.

Extended to hybrid terrestrial-satellite/UAV networks, where the regular cellular structure does not exist, the interference therein is more complex. Liu *et al.* [30] proposed a process-oriented optimization framework and jointly allocated subchannels, transmit power, and hovering time of a UAV swarm. Zhu *et al.* [31] investigated the downlink NOMA for an integrated satellite-terrestrial network. To cancel out inter-group interference, zero-forcing beamforming was applied for both terrestrial and satellite BSs, and a joint power allocation scheme was devised to mitigate the inter-network interference. Moving forward, Lin *et al.* [32] utilized collaborative beamforming to tackle troubling interference and optimized power allocation for sum-rate maximization. Considering the UAV network, Zhao *et al.* [33] investigated the cooperation of the UAV and the TBS. The trajectory of the UAV was jointly optimized with user scheduling to maximize the sum rate of UAV-assisted users under the interference constraint of the TBS. In turn, the NOMA precoding of the TBS was optimized to cancel the interference to UAV-assisted users. Similarly, Peng *et al.* [34] considered a UAV-assisted NOMA network and optimized the user scheduling, UAV trajectory and NOMA precoding.

The above studies provide valuable references to tackle the interference in NOMA-based networks. The superiority of NOMA was proven in various settings. However, the NOMA performance under hybrid satellite-UAV-terrestrial networks has rarely been evaluated, which may be a promising solution to provide on-demand coverage for widely and sparsely distributed maritime IoT. Besides, to cover the wide area of

maritime, facilities in terms of TBSs and UAVs would not stand alone, and designs from the systematical view should be more emphasized. Moreover, present studies mostly assume the full CSI is available for resource scheduling. But for the hybrid satellite-UAV-terrestrial network, acquiring full CSI is not easy. It not only requires the interconnection of space, air, and ground components but also faces the problem of timing and frequency synchronization. In a nutshell, practical regimes to evaluate the NOMA-based hybrid satellite-UAV-terrestrial network for maritime coverage are still lacking.

B. Main Contributions

In this paper, we explore the potential gains of the NOMA-based hybrid satellite-UAV-terrestrial network for maritime coverage enhancement using the unique features of maritime channels and maritime users. We summarize our main contributions as follows.

1) We establish a NOMA-based hybrid satellite-UAV-terrestrial maritime network for on-demand coverage. Tethered UAVs are dispatched to form virtual clusters with TBSs, coordinately serving maritime IoT in a user-centric manner. The NOMA technique is adopted to agilely include various users, so as to accommodate the wide sparsity of maritime IoT. We also consider spectrum sharing between nearshore clusters and maritime satellites. The satellites mainly support far sea areas beyond the coverage of the nearshore network.
2) We formulate an ergodic sum-rate maximization problem with the constraints of the inter-segment interference and the minimal quality-of-service (QoS) requirement. To reduce the system overhead, only large-scale CSI is used for optimization, which could be acquired based on position information. The problem is non-convex with intractable non-linear constraints. We first turn the maximization problem into a max-min problem and then construct monotonous auxiliary functions to get rid of the intractable non-linear constraints. Based on the method of successive convex approximation, the problem is solved in an efficient iterative way.
3) We evaluate the proposed scheme by simulations. It shows that our power allocation scheme is effective in mitigating challenging inter-user, inter-cluster, and inter-segment interference, and the proposed algorithm takes on low computational complexity. The potential gain of the NOMA-based hybrid satellite-UAV-terrestrial network is also shown. It is observed that the nearshore coverage can be enhanced by designed virtual clusters, and the NOMA technique can accommodate the wide sparsity of maritime IoT.

C. Organization and Notation

The rest of this paper is organized as follows. Section II introduces the system model of the hybrid satellite-UAV-terrestrial network. The joint power allocation scheme is shown in Section III, which maximizes the ergodic sum rate with practical constraints. Simulation results and conclusions are presented in Section IV and Section V, respectively.

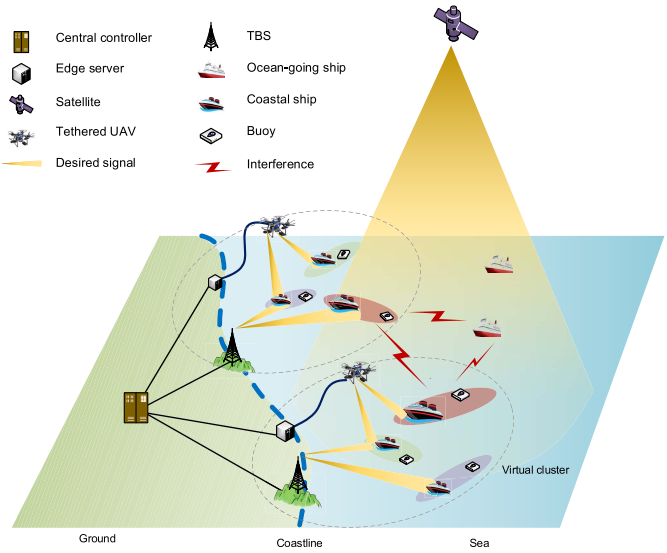

Fig. 1. Illustration of a NOMA-based hybrid satellite-UAV-terrestrial network on the sea, where TBSs and UAVs form virtual clusters in a user-centric manner, and coastal ships and buoys are paired in each virtual cluster. The ocean-going ships are connected by the satellite. In this network, there exists challenging inter-user, inter-cluster, and inter-segment interference.

Throughout this paper, vectors and matrices are represented by lower and upper boldface symbols. $\mathbb{C}^{M\times N}$ represents the set of $M \times N$ complex matrices and $\mathbf{I}_M$ is the unit matrix of $M \times M$. $||\cdot||$ denotes the Euclidean norm and $(\cdot)^H$ is the operation of the transpose conjugate, $\det(\cdot)$ represents the determinant operator. The complex Gaussian distribution of zero mean and σ^2 variance is denoted as $\mathcal{CN}(0,\sigma^2)$. $\mathrm{E}_s(\cdot)$ is the expectation operation with respect to s.

II. System Model

As shown in Fig. 1, we consider a NOMA-based satellite-UAV-terrestrial network on the sea. In nearshore areas, tethered UAVs are dynamically dispatched and form virtual clusters with TBSs for serving users therein. When virtual clusters are formed, we assume that the positions of UAVs are fixed.[1] These clusters can alleviate the site scarcity of TBSs and also extend the coverage scope. To accommodate the wide sparsity of maritime IoT, the NOMA scheme is applied, which provides great flexibility to pair different users. As an example shown in Fig. 1, NOMA is used to offer high-rate services to coastal ships while carrying additional bits for buoys by serving them in pairs. Within a cluster, there are multiple users, and different user pairs are allocated with orthogonal physical resource blocks (PRBs). Since the interference only occurs among the users using the same PRB, we thereby take one PRB and the corresponding users into account. For the areas outside of the nearshore network, marine satellites provide complementary coverage. Edge servers are applied to collect position information, perform cooperation, and provide power supplies for UAVs. They are connected to the central controller, where the cooperative resource allocation is implemented.

[1]In practice, the UAVs should be deployed in an on-demand manner, according to the user distributions.

We assume there are K virtual clusters, and in cluster k ($k = 1, \ldots, K$), two NOMA users equipped with M_k antennas are served by T_k TBSs and U_k UAVs. All TBSs and UAVs are set to have a single antenna. There are also J single-antenna users served by the satellites. They use the same spectrum as NOMA users. When these satellite users move to the nearshore area, they may become NOMA users to share high-rate services. In practice, multi-mode terminals are required for this role shift, which increases the cost of a single marine user.

We consider a composite channel model to depict both small-scale and large-scale fading. Denote $\mathbf{H}_m^{(k,i)} \in \mathbb{C}^{M_k \times (T_i+U_i)}$ as the channel between user m in cluster k and transmitters in cluster i. It is given by

$$\mathbf{H}_m^{(k,i)} = \mathbf{S}_m^{(k,i)} (\mathbf{L}_m^{(k,i)})^{\frac{1}{2}}, \quad m = 1, 2, \quad k = 1, \ldots, K, \quad (1)$$

where $\mathbf{S}_m^{(k,i)} \in \mathbb{C}^{M_k \times (T_i+U_i)}$ is the matrix of small-scale fading whose elements are independently and identically distributed (i.i.d) Gaussian random variables of the $\mathcal{CN}(0, 1)$ distribution. $\mathbf{L}_m^{(k,i)} \in \mathbb{C}^{(T_i+U_i)\times(T_i+U_i)}$ is the diagonal matrix of large-scale fading

$$\mathbf{L}_m^{(k,i)} = \begin{bmatrix} l_{m,1}^{(k,i)} & & \mathbf{O} \\ & \ddots & \\ \mathbf{O} & & l_{m,T_i+U_i}^{(k,i)} \end{bmatrix}, \quad (2)$$

where $l_{m,n}^{(k,i)}, n = 1, .., T_i$, represents the large-scale fading of the TBS link and $l_{m,n}^{(k,i)}$, $n = T_i + 1, .., T_i + U_i$, represents the large-scale fading of the UAV link. For TBSs, we adopt the Hata model, which has been proven to be effective for the maritime environment [35],

$$\begin{aligned} l_{m,n}^{(k,i)}[\text{dB}] = {} & (44.9 - 6.55 \log_{10} h_t) \log_{10} \frac{d_{m,n}^{(k,i)}}{1000} \\ & + (35.46 - 1.1 h_r) \log_{10} f_c - 13.82 \log_{10} h_r \\ & + 0.7 h_r + C + 45.5, \end{aligned} \quad (3)$$

where h_r(m) and h_t(m) represent the height of user terminals and TBSs, respectively, $d_{m,n}^{(k,i)}$(m) is the distance element, f_c(MHz) is the carrier frequency, and C is a constant related to the environment. For UAVs, a model that considers both line-of-sight (LOS) and non-line-of-sight (NLOS) factors is adopted [36]. It is also applicable for the maritime scenario [18],

$$l_{m,n}^{(k,i)}[\text{dB}] = \frac{A}{1 + a e^{-b(\rho_{m,n}^{(k,i)} - a)}} + B_{m,n}^{(k,i)}, \quad (4)$$

where

$$A = \eta_{LOS} - \eta_{NLOS}, \quad (5a)$$

$$B_{m,n}^{(k,i)} = 20 \log_{10}(d_{m,n}^{(k,i)}) + 20 \log_{10}\big(\frac{4\pi f_c}{c}\big) + \eta_{NLOS}, \quad (5b)$$

$$\rho_{m,n}^{(k,i)} = \frac{180}{\pi} \arcsin\big(\frac{h_u}{d_{m,n}^{(k,i)}}\big), \quad (5c)$$

where h_u(m) is the height of UAVs, c is the speed of light, and η_{LOS}, η_{NLOS}, a and b are constants related to the environment. Considering the antenna gains of transmitters and receivers, i.e., g_t[dBi] and g_r[dBi], the total power loss from transmitters to receivers is calculated by

$$l_{m,n}^{(k,i)}[\text{dB}] = l_{m,n}^{(k,i)}[\text{dB}] - g_t[\text{dBi}] - g_r[\text{dBi}]. \quad (6)$$

For further formulations, $l_{m,n}^{(k,i)}[\text{dB}]$ is transformed into $l_{m,n}^{(k,i)}$,

$$l_{m,n}^{(k,i)} = 10^{-\frac{l_{m,n}^{(k,i)}[\text{dB}]}{10}}, \quad m = 1, 2, \quad k, i = 1, \ldots, K. \quad (7)$$

Similarly, the channel from cluster k to satellite user j is given by

$$\mathbf{h}'^{(j,k)} = \mathbf{s}'^{(j,k)} (\mathbf{L}'^{(j,k)})^{\frac{1}{2}}, \quad j = 1, \ldots, J, \quad k = 1, \ldots, K, \quad (8)$$

where $\mathbf{s}'^{(j,k)} \in \mathbb{C}^{1\times(T_k+U_k)}$ denotes the small-scale fading and $\mathbf{L}'^{(j,k)} \in \mathbb{C}^{(T_k+U_k)\times(T_k+U_k)}$ is the large-scale fading, i.e, $\mathbf{L}'^{(j,k)} = \text{diag}\{l_1'^{(j,k)}, \ldots, l_{T_k+U_k}'^{(j,k)}\}$.

From the expressions of (3) and (4), it is easy to find that large-scale fading is highly related to users' and transmitters' positions, while small-scale fading is unpredictable. To avoid the huge overhead, we assume only large-scale CSI is available. The corresponding position data could be obtained from existing monitoring systems such as the Automatic Identification System (AIS) [37].

III. Joint Power Allocation for Sum-Rate Maximization

A. Problem Formulation

Denote $\mathbf{x}^{(k)} \in \mathbb{C}^{(T_k+U_k)\times 1}$ as the downlink signal in cluster k, and it is expressed as

$$\mathbf{x}^{(k)} = \mathbf{x}_1^{(k)} + \mathbf{x}_2^{(k)}, \quad k = 1, \ldots, K, \quad (9)$$

with $\mathbf{x}_1^{(k)}$ and $\mathbf{x}_2^{(k)}$ representing the transmit signals of user 1 and user 2. The received signals are given by

$$\begin{aligned} \mathbf{y}_1^{(k)} = {} & \mathbf{H}_1^{(k,k)} \mathbf{x}_1^{(k)} + \mathbf{H}_1^{(k,k)} \mathbf{x}_2^{(k)} \\ & + \sum_{i=1, i\neq k}^{K} \mathbf{H}_1^{(k,i)} \mathbf{x}^{(i)} + \mathbf{n}_1^{(k)}, \end{aligned} \quad (10a)$$

$$\begin{aligned} \mathbf{y}_2^{(k)} = {} & \mathbf{H}_2^{(k,k)} \mathbf{x}_2^{(k)} + \mathbf{H}_2^{(k,k)} \mathbf{x}_1^{(k)} \\ & + \sum_{i=1, i\neq k}^{K} \mathbf{H}_2^{(k,i)} \mathbf{x}^{(i)} + \mathbf{n}_2^{(k)}, \end{aligned} \quad (10b)$$

where $\mathbf{n}_m^{(k)} \in \mathbb{C}^{M_k \times 1}$ $(m = 1, 2)$ represents the additive white Gaussian noise of $\mathcal{CN}(0, \sigma^2 \mathbf{I}_{M_k})$ distribution.

Without loss of generality, we assume user 1 is the user who implements the SIC. When receiving the message, user 1 first decodes the content of user 2 and removes it from the received signal, subsequently decoding its own message. After SIC, the covariance matrix of interference plus noise of user 1 in cluster k is given by

$$\begin{aligned} \bar{\mathbf{Z}}_1^{(k)} = {} & \mathbf{E}_{\mathcal{S}}\big[\sum_{i=1, i\neq k}^{K} \mathbf{H}_1^{(k,i)} \mathbf{P}^{(i)} \mathbf{H}_1^{(k,i)^H} + \sigma^2 \mathbf{I}_{M_k} \big], \\ = {} & \big(\sum_{i=1, i\neq k}^{K} \sum_{n=1}^{T_i+U_i} l_{1,n}^{(k,i)} P_n^{(i)} + \sigma^2 \big) \mathbf{I}_{T_k+U_k}, \end{aligned} \quad (11)$$

where $\mathbf{E}_{\mathcal{S}}$ is the expectation operator over small-scale fading and $\mathcal{S} = \{\mathbf{S}_m^{(k,i)} | m = 1,2\ k, i = 1,\ldots,K\}$ is the set of the small-scale fading. $\mathbf{P}^{(i)}$ is the power matrix of cluster i, i.e, $\mathbf{P}^{(i)} = \text{diag}\{P_1^{(i)},\ldots,P_{T_i+U_i}^{(i)}\}$, which includes the power of user 1 and 2, i.e., $\mathbf{P}^{(i)} = \mathbf{P}_1^{(i)} + \mathbf{P}_2^{(i)}$ with $\mathbf{P}_m^{(i)} = \text{diag}\{P_{m,1}^{(i)},\ldots,P_{m,T_i+U_i}^{(i)}\},\ m = 1,2$. The above equation is obtained based on the assumption of white Gaussian interference, which would yield a lower bound of the actual capacity [38]. For express convenience, we denote $\sigma_{k,1}^2(\mathbf{P})$ as the sum noise suffered by user 1,

$$\sigma_{k,1}^2(\mathbf{P}) \triangleq \underbrace{\sum_{i=1,i\neq k}^{K}\sum_{n=1}^{T_i+U_i} l_{1,n}^{(k,i)} P_n^{(i)}}_{\text{inter-cluster interference}} + \sigma^2, \tag{12}$$

where $\mathbf{P}$ is the set of transmit power in each cluster, i.e., $\mathbf{P} = \{\mathbf{P}^{(i)} | i = 1,\ldots,K\}$.

As for user 2, it regards user 1's signal as the background noise and directly decodes its own message. Suffering from both inter-cluster and inter-user interference, the interference plus noise of user 2 is calculated by

$$\sigma_{k,2}^2(\mathbf{P}) = \underbrace{\sum_{i=1,i\neq k}^{K}\sum_{n=1}^{T_i+U_i} l_{2,n}^{(k,i)} P_n^{(i)}}_{\text{inter-cluster interference}} + \underbrace{\sum_{n=1}^{T_k+U_k} l_{2,n}^{(k,k)} P_{1,n}^{(k)}}_{\text{inter-user interference}} + \sigma^2. \tag{13}$$

When only large-scale CSI is known at transmitters, the ergodic sum rate of nearshore clusters is of great importance to the network,

$$\bar{R}(\mathbf{P}) = \sum_{k=1}^{K}\sum_{m=1}^{2} \bar{R}_{k,m}(\mathbf{P}), \tag{14}$$

where

$$\bar{R}_{k,m}(\mathbf{P}) = \mathbf{E}_{\mathcal{S}}\left[\log_2 \det\left(\mathbf{I}_{M_k} + \frac{\mathbf{H}_m^{(k,k)}\mathbf{P}_m^{(k)}\mathbf{H}_m^{(k,k)^H}}{\sigma_{k,m}^2(\mathbf{P})}\right)\right] \tag{15}$$

is the ergodic rate of user m in cluster k.

To ensure the NOMA principle is applicable, user 1 should be capable of decoding the message of user 2. In other words, the rate that user 1 receives the message of user 2, i.e., $\bar{R}_{k,1\to 2}(\mathbf{P})$ should be greater than user 2's own rate. This condition is expressed as

$$\bar{R}_{k,2}(\mathbf{P}) \leqslant \bar{R}_{k,1\to 2}(\mathbf{P}), \quad k = 1,\ldots,K, \tag{16}$$

where $\bar{R}_{k,1\to 2}(\mathbf{P})$ is given by

$$\bar{R}_{k,1\to 2}(\mathbf{P}) = \mathbf{E}_{\mathcal{S}}\left[\log_2 \det\left(\mathbf{I}_{M_k} + \frac{\mathbf{H}_1^{(k,k)}\mathbf{P}_2^{(k)}\mathbf{H}_1^{(k,k)^H}}{\sigma_{k,1\to 2}^2(\mathbf{P})}\right)\right], \tag{17}$$

$$\sigma_{k,1\to 2}^2(\mathbf{P}) = \underbrace{\sum_{i=1,i\neq k}^{K}\sum_{n=1}^{T_i+U_i} l_{1,n}^{(k,i)} P_n^{(i)}}_{\text{inter-cluster interference}} + \underbrace{\sum_{n=1}^{T_k+U_k} l_{1,n}^{(k,k)} P_{1,n}^{(k)}}_{\text{inter-user interference}} + \sigma^2. \tag{18}$$

It can be proven that (16) holds if user 1 has the better effective channel. But for the considered network, link qualities are influenced by inter-cluster interference, which can not be known before power allocation. To achieve the optimum, user orders are expected to be jointly optimized with power allocation. Considerable gains can be achieved if we take both user pairing and resource allocation into account [39]. For simplicity, in this paper, we consider a special case in which user 1 and user 2 are separated by a large distance. The distinct large-scale fading of two users guarantees that no matter how the power is allocated, user 1 always occupies better channel conditions. Thus, the user order is predefined in this paper before power allocation. This assumption also accords with the wide sparsity of maritime IoT.

Since we assume user 1 possesses better channels, traditional opportunistic schemes tend to give more resources to user 1 to maximize the efficiency. This greatly influences the fairness of the network. Therefore, taking user fairness into account, we impose the constraint of the basic QoS requirement of user 2, i.e., r_k,

$$\bar{R}_{k,2}(\mathbf{P}) \geqslant r_k, \quad k = 1,\ldots,K. \tag{19}$$

Furthermore, satellite users suffer from inter-segment interference due to spectrum sharing. To avoid potential impairment, the leakage power from nearshore clusters is restricted not to exceed the maximum tolerable interference of satellite receivers, i.e., $\bar{P}$,

$$\sum_{k=1}^{K} \mathbf{E}_{\mathbf{s}'} \parallel \mathbf{h}'^{(j,k)}\mathbf{P}^{(k)}\mathbf{h}'^{(j,k)^H} \parallel \leqslant \bar{P}, \quad j = 1,\ldots,J, \tag{20}$$

where $\mathbf{s}' = \{\mathbf{s}'^{(j,k)} | j = 1,\ldots,J, k = 1,\ldots,K\}$. Based on the Gaussian distribution of $\mathbf{s}'$, the left side of (20) can be simplified as

$$\sum_{k=1}^{K} \mathbf{E}_{\mathbf{s}'} \parallel \mathbf{h}'^{(j,k)}\mathbf{P}^{(k)}\mathbf{h}'^{(j,k)^H} \parallel = \sum_{k=1}^{K}\sum_{n=1}^{T_k+U_k} l'^{(j,k)}_n P_n^{(k)}. \tag{21}$$

Generally, the nearshore network also suffers from interference from the satellite, but this impact is much smaller compared with strong inter-cluster and inter-user interference and we neglect it in this paper.

With the consideration of the QoS requirement (19), inter-segment interference (20) and practical power constraints, we aim to maximize the ergodic sum rate of the nearshore network based on the large-scale CSI.

$$\text{(P1)} \quad \max_{\mathbf{P}} \ \bar{R}(\mathbf{P}) \tag{22a}$$

$$s.t. \quad \bar{R}_{k,2}(\mathbf{P}) \geqslant r_k \tag{22b}$$

$$\mathbf{P}^{(k)} \succeq 0 \tag{22c}$$

$$\text{tr}(\mathbf{P}^{(k)}) \leqslant P_{\max} \tag{22d}$$

$$P_n^{(k)} \leqslant P_{\text{Tmax}}, \quad n = 1,\ldots,T_k \tag{22e}$$

$$P_n^{(k)} \leqslant P_{\text{Umax}}, \quad n = T_k+1,\ldots,T_k+U_k \tag{22f}$$

$$\sum_{k=1}^{K}\sum_{n=1}^{T_k+U_k} P_n^{(k)} l'^{(j,k)}_n \leqslant \bar{P}, \quad j=1,\ldots,J \tag{22g}$$

$$k=1,\ldots,K,$$

where P_{Tmax} and P_{Umax} are the maximum affordable transmit power of the TBSs and UAVs, and $P_{\max}$ is the power budget of each cluster.

In practical implementation, satellite users take charge of the estimation of $\bar{P}$, which is obtained based on the receiver sensitivity. When satellite users approach to the nearshore region and sense that they may be interfered, they would inform the satellites of this parameter. The satellite system periodically reports $\bar{P}$ accompanied by satellite user locations to the central controller. Afterwards, the central controller calculates the large-scale CSI of the link from TBSs/UAVs to nearshore users/satellite users. This can be done by a prior database, i.e., radio map [40]. On this basis, the proposed power allocation scheme is executed in the central controller to maximize the coverage performance of nearshore clusters while ensuring peaceful coexistence between nearshore and satellite networks. As a result, the nearshore network and satellites actually work in a loosely coordinated manner. The two parts only share positions and the troubling CSI estimation is bypassed. These traits are friendly to practical implementation for the restricted conditions in reality.

In addition, the proposed model is also applicable to multi-user NOMA. In this case, the interference plus noise of user m $(m \geqslant 2)$ should take the signals from user 1 to user $m-1$ into account, i.e, $\sigma^2_{k,m}(\mathbf{P}) = \sum_{i=1,i\neq k}^{K}\sum_{n=1}^{T_i+U_i} l^{(k,i)}_{m,n} P_n^{(i)} + \sum_{n=1}^{T_k+U_k}\sum_{o=1}^{m-1} l^{(k,k)}_{m,n} P^{(k)}_{o,n} + \sigma^2$, and the SIC condition (16) should hold for any user pair (m_1, m_2) in the same cluster, i.e., $\bar{R}_{k,m_2}(\mathbf{P}) \leqslant \bar{R}_{k,m_1\to m_2}(\mathbf{P})$ for any $m_2 > m_1$. In addition, the QoS constraint (22b) should take user $2 \sim m$ into account. However, due to the implementation complexity and the strict SIC condition, the two-user NOMA is more friendly for practical applications [24], [26], [31]. Out of this concern, we focus on two-user NOMA in this paper and leave the multi-user NOMA for future studies.

(P1) is complex due to the non-convex objective and the non-convex feasible set. The ergodic rate is trapped in expectation operations, leading to a no closed-form expression. To tackle this problem, the tricky expectations should be removed first. By referring to [41], an approximation of $\bar{R}_{k,m}(\mathbf{P})$ is introduced as follows

$$\bar{R}_{k,m}(\mathbf{P}) \approx g_{k,m}(\mathbf{P}, v^*_{k,m}) \tag{23a}$$

$$= \sum_{n=1}^{T_k+U_k} \log_2\left(1+\frac{M_k l^{(k,k)}_{m,n} P^{(k)}_{m,n}}{v^*_{k,m}\sigma^2_{k,m}(\mathbf{P})}\right) \tag{23b}$$

$$+ M_k \log_2 v^*_{k,m} - M_k \log_2(e)[1-(v^*_{k,m})^{-1}],$$

where $v^*_{k,m}$ is given by

$$v^*_{k,m} = 1 + \sum_{n=1}^{T_k+U_k} \frac{l^{(k,k)}_{m,n} P^{(k)}_{m,n}}{\sigma^2_{k,m}(\mathbf{P}) + M_k l^{(k,k)}_{m,n} P^{(k)}_{m,n} (v^*_{k,m})^{-1}}. \tag{24}$$

This approximation is derived in the asymptotic case when the antenna number goes to infinity. In this situation, the variance profile of the random channel converges to a limit bound. Under this condition, the Shannon transform [42] of the asymptotic spectrum of the variance profile could be applied to remove the expectation operation. On this basis, the approximate closed-form expression could be obtained [43]. This approximation has been proven to be quite accurate even with several antennas [41]. The detailed proof of this approximation is however out of the scope of this paper. Readers could refer [41]–[43] for more detailed discussions.

Then, the original problem (P1) is recast into (P2) as follows

$$\text{(P2)} \quad \max_{\mathbf{P}} \; g(\mathbf{P}, \mathbf{v}^*) \tag{25a}$$

$$s.t. \quad g_{k,2}(\mathbf{P}, v^*_{k,2}) \geqslant r_k \tag{25b}$$

$$v^*_{k,m} = 1 + \sum_{n=1}^{T_k+U_k} \frac{l^{(k,k)}_{m,n} P^{(k)}_{m,n}}{\sigma^2_{k,m}(\mathbf{P}) + M_k l^{(k,k)}_{m,n} P^{(k)}_{m,n} (v^*_{k,m})^{-1}} \tag{25c}$$

$$\mathbf{P}^{(k)} \succeq 0 \tag{25d}$$

$$\text{tr}(\mathbf{P}^{(k)}) \leqslant P_{\max} \tag{25e}$$

$$P_n^{(k)} \leqslant P_{\text{Tmax}}, \quad n=1,\ldots,T_k \tag{25f}$$

$$P_n^{(k)} \leqslant P_{\text{Umax}}, \quad n=T_k+1,\ldots,T_k+U_k \tag{25g}$$

$$\sum_{k=1}^{K}\sum_{n=1}^{T_k+U_k} P_n^{(k)} l'^{(j,k)}_n \leqslant \bar{P}, \quad j=1,\ldots,J \tag{25h}$$

$$m=1,2 \quad \text{and} \quad k=1,\ldots,K,$$

where $g(\mathbf{P}, \mathbf{v}^*) = \sum_{k=1}^{K}\sum_{m=1}^{2} g_{k,m}(\mathbf{P}, v^*_{k,m})$ and $\mathbf{v}^* = \{v^*_{k,m} | m=1,2,\ k=1,\ldots,K\}$. Although we get rid of the expectation operations in (P2), the introduced implicit parameter $\mathbf{v}^*$ with an extra group of complex non-linear constraints (25c) brings great troubles. The objective (25a) and QoS constraint (25b) are both coupled with $\mathbf{v}^*$ in a non-convex form, which makes this problem difficult to tackle. To eliminate these non-linear constraints, we apply the max-min method and the auxiliary function method for the objective and QoS constraint (25b), respectively.

B. An Equivalent Max-Min Problem

By analyzing the monotonicity of $g_{k,m}(\mathbf{P}, v_{k,m})$, we find that $g_{k,m}(\mathbf{P}, v_{k,m})$ is monotonically decreasing in $[1, v^*_{k,m})$ and monotonically increasing in $[v^*_{k,m}, +\infty)$ [41]. This means $v^*_{k,m}$ is the minimal point of $g_{k,m}(\mathbf{P}, v_{k,m})$, i.e.,

$$g_{k,m}(\mathbf{P}, v^*_{k,m}) = \min_{v_{k,m}\geqslant 1} g_{k,m}(\mathbf{P}, v_{k,m}). \tag{26}$$

Based on (26), we thus recast (P2) into a max-min problem as

$$\begin{aligned}
(\text{P3}) \max_{\mathbf{P}} \ \min_{\mathbf{v}} \ & g(\mathbf{P},\mathbf{v}) && (27a)\\
s.t. \quad & g_{k,2}(\mathbf{P},v_{k,2}^*) \geqslant r_k && (27b)\\
& v_{k,2}^* = 1+\sum_{n=1}^{T_k+U_k} \frac{l_{2,n}^{(k,k)}P_{2,n}^{(k)}}{\sigma_{k,2}^2(\mathbf{P})+M_k l_{2,n}^{(k,k)}P_{2,n}^{(k)}(v_{k,2}^*)^{-1}} && (27c)\\
& v_{k,m} \geqslant 1 && (27d)\\
& \mathbf{P}^{(k)} \succeq 0 && (27e)\\
& \mathrm{tr}(\mathbf{P}^{(k)}) \leqslant P_{\max} && (27f)\\
& P_n^{(k)} \leqslant P_{\text{Tmax}}, \quad n=1,\ldots,T_k && (27g)\\
& P_n^{(k)} \leqslant P_{\text{Umax}}, \quad n=T_k+1,\ldots,T_k+U_k && (27h)\\
& \sum_{k=1}^{K}\sum_{n=1}^{T_k+U_k} P_n^{(k)} l'^{(j,k)}_n \leqslant \bar{P}, \quad j=1,\ldots,J && (27i)\\
& m=1,2 \ \text{ and } \ k=1,\ldots,K,
\end{aligned}$$

where the optimal solution $(\mathbf{P}^*,\mathbf{v}^*)$ would be the saddle point of $g(\mathbf{P},\mathbf{v})$.

C. Simplification of the Non-Linear Constraint

To eliminate the fixed-point $v_{k,2}^*$ in the QoS constraint, we first construct an auxiliary function, i.e., $f_k(\mathbf{P},z_k)$ as follows

$$\begin{aligned}
f_k(\mathbf{P},z_k) = & \sum_{n=1}^{T_k+U_k}\Bigg(\log_2\big(1+\frac{M_k l_{2,n}^{(k,k)}P_{2,n}^{(k)}}{z_k\sigma_{k,2}^2(\mathbf{P})}\big)\\
& -\frac{\log_2(e)M_k l_{2,n}^{(k,k)}P_{2,n}^{(k)}}{z_k\sigma_{k,2}^2(\mathbf{P})+M_k l_{2,n}^{(k,k)}P_{2,n}^{(k)}}\Bigg)\\
& +M_k\log_2 z_k. \qquad (28)
\end{aligned}$$

Theorem 1: Under the condition that $M_k \geqslant T_k+U_k$, $f_k(\mathbf{P},z_k)$ is monotonically increasing with respect to z_k. The relationship between $g_{k,2}(\mathbf{P},v_{k,2}^*)$ and $f_k(\mathbf{P},z_k)$ is given by

$$g_{k,2}(\mathbf{P},v_{k,2}^*) = \max_{1\leqslant z_k\leqslant v_{k,2}^*} f_k(\mathbf{P},z_k). \qquad (29)$$

Proof: See Appendix A.

According to theorem 1, the QoS constraint (27b) can be recast into

$$\max_{1\leqslant z_k\leqslant v_{k,2}^*} f_k(\mathbf{P},z_k) \geqslant r_k \Rightarrow \begin{cases} f_k(\mathbf{P},z_k)\geqslant r_k,\\ 1\leqslant z_k\leqslant v_{k,2}^*. \end{cases} \qquad (30)$$

To further simplify $z_k \leqslant v_{k,2}^*$, we note that (27c) can be equivalently rewritten as

$$(v_{k,2}^*)^{-1}+\sum_{n=1}^{T_k+U_k}\frac{l_{2,n}^{(k,k)}P_{2,n}^{(k)}}{v_{k,2}^*\sigma_{k,2}^2(\mathbf{P})+M_k l_{2,n}^{(k,k)}P_{2,n}^{(k)}}=1. \qquad (31)$$

As $(z_k)^{-1}+\sum_{n=1}^{T_k+U_k}\frac{l_{2,n}^{(k,k)}P_{2,n}^{(k)}}{z_k\sigma_{k,2}^2(\mathbf{P})+M_k l_{2,n}^{(k,k)}P_{2,n}^{(k)}}$ is monotonically decreasing with z_k, so, for any $z_k\geqslant 0$, we have that

$$z_k \leqslant v_{k,2}^* \Rightarrow (z_k)^{-1}+\sum_{n=1}^{T_k+U_k}\frac{l_{2,n}^{(k,k)}P_{2,n}^{(k)}}{z_k\sigma_{k,2}^2(\mathbf{P})+M_k l_{2,n}^{(k,k)}P_{2,n}^{(k)}}\geqslant 1. \qquad (32)$$

Based on (30) and (32), (P3) is further recast into (P4),

$$\begin{aligned}
(\text{P4}) \ \max_{\mathbf{P},z_k} \ \min_{\mathbf{v}} \ & g(\mathbf{P},\mathbf{v}) && (33a)\\
s.t. \quad & f_k(\mathbf{P},z_k)\geqslant r_k && (33b)\\
& (z_k)^{-1}+\sum_{n=1}^{T_k+U_k}\frac{l_{2,n}^{(k,k)}P_{2,n}^{(k)}}{z_k\sigma_{k,2}^2(\mathbf{P})+M_k l_{2,n}^{(k,k)}P_{2,n}^{(k)}}\geqslant 1 && (33c)\\
& v_{k,m}\geqslant 1, z_k\geqslant 1 && (33d)\\
& \mathbf{P}^{(k)}\succeq 0 && (33e)\\
& \mathrm{tr}(\mathbf{P}^{(k)})\leqslant P_{\max} && (33f)\\
& P_n^{(k)}\leqslant P_{\text{Tmax}}, \quad n=1,\ldots,T_k && (33g)\\
& P_n^{(k)}\leqslant P_{\text{Umax}}, \quad n=T_k+1,\ldots,T_k+U_k && (33h)\\
& \sum_{k=1}^{K}\sum_{n=1}^{T_k+U_k} P_n^{(k)} l'^{(j,k)}_n \leqslant \bar{P}, \quad j=1,\ldots,J && (33i)\\
& m=1,2 \text{ and } k=1,\ldots,K.
\end{aligned}$$

Taking a further look of $f_k(\mathbf{P},z_k)$, it can be reorganized as

$$\begin{aligned}
f_k(\mathbf{P},z_k) = & -\log_2(e)\sum_{n=1}^{T_k+U_k}\Bigg(\frac{M_k l_{2,n}^{(k,k)}P_{2,n}^{(k)}}{z_k\sigma_{k,2}^2(\mathbf{P})+M_k l_{2,n}^{(k,k)}P_{2,n}^{(k)}}\\
& +\mathrm{In}\big(1-\frac{M_k l_{2,n}^{(k,k)}P_{2,n}^{(k)}}{z_k\sigma_{k,2}^2(\mathbf{P})+M_k l_{2,n}^{(k,k)}P_{2,n}^{(k)}}\big)\Bigg)\\
& +M_k\log_2 z_k, \qquad (34)
\end{aligned}$$

where the fraction term, i.e., $\frac{M_k l_{2,n}^{(k,k)}P_{2,n}^{(k)}}{z_k\sigma_{k,2}^2(\mathbf{P})+M_k l_{2,n}^{(k,k)}P_{2,n}^{(k)}}$, is the same. Motivated by this, we introduce a group of slack variables, i.e., $\mathbf{t}_k=\{t_{k,n}|n=1,\ldots,T_k+U_k\}$, and transform the auxiliary function, i.e., $f_k(\mathbf{P},z_k)$, as follows,

$$\begin{aligned}
\mathcal{F}_k(z_k,\mathbf{t}_k) = & -\log_2(e)\sum_{n=1}^{T_k+U_k}\big(t_{k,n}+\mathrm{In}\big(1-t_{k,n}\big)\big)\\
& +M_k\log_2 z_k, \quad k=1,\ldots,K, \qquad (35)
\end{aligned}$$

where $t_{k,n}$ corresponds to the fraction term in $f_k(\mathbf{P},z_k)$. Based on the increasing monotonicity of $-[x+\mathrm{In}(1-x)]$, it is clear that $\mathcal{F}_k(z_k,\mathbf{t}_k)$ is monotonically increasing with $\mathbf{t}_k$. Therefore, the QoS constraint can be further converted into (36), as shown at the bottom of the next page.

Problem (P4) is turned into (P5) as,

$$\begin{aligned}
(\text{P5}) \ \max_{\mathbf{P},z_k,\mathbf{t}_k} \ \min_{\mathbf{v}} \ & g(\mathbf{P},\mathbf{v}) && (37a)\\
s.t. \quad & \mathcal{F}_k(z_k,\mathbf{t}_k)\geqslant r_k && (37b)\\
& (z_k)^{-1}+\frac{1}{M_k}\sum_{n=1}^{T_k+U_k} t_{k,n}\geqslant 1 && (37c)
\end{aligned}$$

$$t_{k,n} \leqslant \frac{M_k l_{2,n}^{(k,k)} P_{2,n}^{(k)}}{z_k \sigma_{k,2}^2(\mathbf{P}) + M_k l_{2,n}^{(k,k)} P_{2,n}^{(k)}} \tag{37d}$$

$$v_{k,m} \geqslant 1, \quad z_k \geqslant 1, \quad t_{k,n} \geqslant 0 \tag{37e}$$

$$\mathbf{P}^{(k)} \succeq 0 \tag{37f}$$

$$\mathrm{tr}(\mathbf{P}^{(k)}) \leqslant P_{\max} \tag{37g}$$

$$P_n^{(k)} \leqslant P_{\text{Tmax}}, \quad n = 1, \ldots, T_k \tag{37h}$$

$$P_n^{(k)} \leqslant P_{\text{Umax}}, \quad n = T_k + 1, \ldots, T_k + U_k \tag{37i}$$

$$\sum_{k=1}^{K} \sum_{n=1}^{T_k+U_k} P_n^{(k)} l'^{(j,k)}_n \leqslant \bar{P}, \quad j = 1, \ldots, J \tag{37j}$$

$$m = 1, 2, \quad n = 1, \ldots, T_k + U_k, \quad k = 1, \ldots, K.$$

It is noted that if constraint (25b) in (P2) is tight, the optimal solution of (P5) is obtained if and only if constraint (37b) is rightly satisfied when $\mathcal{F}_k(z_k, \mathbf{t}_k)$ reaches its maximum. This means that constraints (37b), (37c) and (37d) are satisfied in the equality condition, i.e., $z_k = v_{2,k}^*$, $t_{k,n} = \frac{M_k l_{2,n}^{(k,k)} P_{2,n}^{(k)}}{z_k \sigma_{k,2}^2(\mathbf{P}) + M_k l_{2,n}^{(k,k)} P_{2,n}^{(k)}}$, and $\mathcal{F}_k(z_k, \mathbf{t}_k) = g_{k,2}(\mathbf{P}, v_{k,2}^*)$. Therefore, we could draw the following lemma.

Lemma 1: The optimal solution of (P5) is the optimal solution of (P2) and vice versa.

Proof: See Appendix B.

Observing (P5), the objective function is still non-convex with respect to $\mathbf{P}$ and $\mathbf{v}$, and constraint (37d) is shown in a complex fraction form. Proceeding with these problems, we first introduce a group of variables $\mathbf{w} = \{w_{k,m} | m = 1, 2, \ k = 1, \ldots, K\}$, which is denoted as $e^{w_{k,m}} = v_{k,m}$. The quasi-convex function $g(\mathbf{P}, \mathbf{v})$ with respect to $\mathbf{v}$ is then transformed into a convex function $\mathcal{G}(\mathbf{P}, \mathbf{w})$ with respect to $\mathbf{w}$, which is given by

$$\mathcal{G}(\mathbf{P}, \mathbf{w}) = \sum_{k=1}^{K} \sum_{m=1}^{2} \mathcal{G}_{k,m}(\mathbf{P}, w_{k,m}), \tag{38}$$

where

$$\mathcal{G}_{k,m}(\mathbf{P}, w_{k,m}) = \sum_{n=1}^{T_k+U_k} \log_2 \left(1 + \frac{M_k l_{m,n}^{(k,k)} P_{m,n}^{(k)}}{e^{w_{k,m}} \sigma_{k,m}^2(\mathbf{P})}\right) + M_k \log_2(e)[w_{k,m} + e^{-w_{k,m}} - 1]. \tag{39}$$

In addition, $\mathcal{G}_{k,m}(\mathbf{P}, w_{k,m})$ can be reorganized into the subtraction of two parts

$$\mathcal{G}_{k,m}(\mathbf{P}, w_{k,m}) = \mathcal{G}_{k,m,1}(\mathbf{P}, w_{k,m}) - \mathcal{G}_{k,m,2}(\mathbf{P}), \tag{40}$$

where

$$\mathcal{G}_{k,m,1}(\mathbf{P}, w_{k,m}) = \sum_{n=1}^{T_k+U_k} \log_2 \left(\sigma_{k,m}^2(\mathbf{P}) + \frac{M_k l_{m,n}^{(k,k)} P_{m,n}^{(k)}}{e^{w_{k,m}}}\right) + M_k \log_2(e)[w_{k,m} + e^{-w_{k,m}} - 1], \tag{41a}$$

$$\mathcal{G}_{k,m,2}(\mathbf{P}) = (T_k + U_k) \log_2 \left(\sigma_{k,m}^2(\mathbf{P})\right). \tag{41b}$$

They are both concave with respect to $\mathbf{P}$. To decouple different variables in (37d), the logarithmic operation is applied. Then, this constraint is reorganized as

$$\mathrm{In}\left(M_k P_{2,n}^{(k)} l_{2,n}^{(k,k)}\right) + \mathrm{In}(1 - t_{k,n}) \geqslant \mathrm{In}(z_k) + \mathrm{In}(t_{k,n}) + \mathrm{In}(\sigma_{k,2}^2(\mathbf{P})). \tag{42}$$

Consequently, based on (38) and (42), we move to (P6) as follows

$$\text{(P6)} \quad \max_{\mathbf{P}, z_k, \mathbf{t}_k} \min_{\mathbf{w}} \ \mathcal{G}(\mathbf{P}, \mathbf{w}) \tag{43a}$$

$$s.t. \quad \mathcal{F}_k(z_k, \mathbf{t}_k) \geqslant r_k \tag{43b}$$

$$(z_k)^{-1} + \frac{1}{M_k} \sum_{n=1}^{T_k+U_k} t_{k,n} \geqslant 1 \tag{43c}$$

$$\mathrm{In}\left(M_k P_{2,n}^{(k)} l_{2,n}^{(k,k)}\right) + \mathrm{In}(1 - t_{k,n}) \geqslant \mathrm{In}(z_k) + \mathrm{In}(t_{k,n}) + \mathrm{In}(\sigma_{k,2}^2(\mathbf{P})) \tag{43d}$$

$$w_{k,m} \geqslant 0, z_k \geqslant 1, t_{k,n} \geqslant 0 \tag{43e}$$

$$\mathbf{P}^{(k)} \succeq 0 \tag{43f}$$

$$\mathrm{tr}(\mathbf{P}^{(k)}) \leqslant P_{\max} \tag{43g}$$

$$P_n^{(k)} \leqslant P_{\text{Tmax}}, \quad n = 1, \ldots, T_k \tag{43h}$$

$$P_n^{(k)} \leqslant P_{\text{Umax}}, \quad n = T_k + 1, \ldots, T_k + U_k \tag{43i}$$

$$\Rightarrow \begin{cases} f_k(\mathbf{P}, z_k) \geqslant r_k, \\ (z_k)^{-1} + \sum_{n=1}^{T_k+U_k} \frac{l_{2,n}^{(k,k)} P_{2,n}^{(k)}}{z_k \sigma_{k,2}^2(\mathbf{P}) + M_k l_{2,n}^{(k,k)} P_{2,n}^{(k)}} \geqslant 1, \quad z_k \geqslant 1, \end{cases}$$

$$\Rightarrow \begin{cases} \mathcal{F}_k(z_k, \mathbf{t}_k) \geqslant r_k, \\ (z_k)^{-1} + \frac{1}{M_k} \sum_{n=1}^{T_k+U_k} t_{k,n} \geqslant 1, \qquad z_k \geqslant 1, \\ t_{k,n} \leqslant \frac{M_k l_{2,n}^{(k,k)} P_{2,n}^{(k)}}{z_k \sigma_{k,2}^2(\mathbf{P}) + M_k l_{2,n}^{(k,k)} P_{2,n}^{(k)}}, \quad t_{k,n} \geqslant 0. \end{cases} \tag{36}$$

Algorithm 1 Iterative Power Allocation Algorithm

Input: $P_{\max}$, P_{Tmax}, P_{Umax}, $\bar{P}$, r_k $(k=1,\ldots,K)$

Initialization: set $\epsilon = 1\times10^{-3}$, $(P^{(k)})^0 = P_{\max}$, $(P_n^{(k)})^0 = \frac{(P^{(k)})^0}{T_k+U_k}$, $n=1,\ldots,T_k+U_k$ and $k=1,..,K$.
for $j=1\sim J$ **do**
  while $(\sum_{k=1}^{K}\sum_{n=1}^{T_k+U_k} l'^{(j,k)}_n (P_n^{(k)})^0 > \bar{P})$ **do**
    $(P^{(k)})^0 = (1-\epsilon)(P^{(k)})^0$;
    $(P_n^{(k)})^0 = \frac{(P^{(k)})^0}{T_k+U_k}$, $n=1,\ldots,T_k+U_k, k=1,\ldots,K$;
  end while
end for
for $k=1\sim K, n=1\sim T_k$ **do**
  if $((P_n^{(k)})^0 > P_{\text{Tmax}})$ **then**
    $(P_n^{(k)})^0 = P_{\text{Tmax}}$;
  end if
end for
for $k=1\sim K, n=T_k+1\sim T_k+U_k$ **do**
  if $((P_n^{(k)})^0 > P_{\text{Umax}})$ **then**
    $(P_n^{(k)})^0 = P_{\text{Umax}}$;
  end if
end for
$(P_{m,n}^{(k)})^0 = \frac{(P_n^{(k)})^0}{2}$, $m=1,2$, $n=1,\ldots,T_k+U_k$, and $k=1,\ldots,K$,
Calculate z_k^0, $\mathbf{t}_k^0$ $(k=1,\ldots,K)$ based on (37c) and (37d) under the equality condition.
Iterations: $s=1,2,\ldots,$
repeat
  Update $\mathbf{P}^s$, $\mathbf{t}_k^s$ and z_k^s $(k=1,\ldots,K)$ by solving (P7);
until $\frac{|\mathcal{G}(\mathbf{P}^s,\mathbf{w}^s)-\mathcal{G}(\mathbf{P}^{s-1},\mathbf{w}^{s-1})|}{\mathcal{G}(\mathbf{P}^{s-1},\mathbf{w}^{s-1})} \leqslant \epsilon$.
Output: $\mathbf{P}^s$.

$$\sum_{k=1}^{K}\sum_{n=1}^{T_k+U_k} P_n^{(k)} l'^{(j,k)}_n \leqslant \bar{P}, \quad j=1,\ldots,J \tag{43j}$$
$$m=1,2, \quad n=1,\ldots,T_k+U_k, \quad k=1,\ldots,K.$$

Up to now, all the separate terms in (P6) are shown in convex or concave forms so that the method of successive convex approximation could be applied. Specifically, in iteration s $(s=1,2,\ldots)$, $\mathcal{G}_{k,m,2}(\mathbf{P})$ in (43a), $\log_2(1-t_{k,n})$ in (43b), $(z_k)^{-1}$ in (43c), and $\ln(z_k)+\ln(t_{k,n})+\ln(\sigma_{k,2}^2(\mathbf{P}))$ in (43d) are linearized by their first-order Taylor expansions at points $\mathbf{P}^{s-1}$, z_k^{s-1} and $\mathbf{t}_k^{s-1}$. Then, the convex problem of iteration s can be formulated as

$$\text{(P7)} \quad \max_{\mathbf{P},z_k,\mathbf{t}_k} \min_{\mathbf{w}} \ \mathcal{G}(\mathbf{P},\mathbf{w}|\mathbf{P}^{s-1}) \tag{44a}$$
$$s.t. \quad \mathcal{F}_k(z_k,\mathbf{t}_k|\mathbf{t}_k^{s-1}) \geqslant r_k \tag{44b}$$
$$-\frac{z_k}{(z_k^{s-1})^2}+\frac{2}{z_k^{s-1}}+\frac{1}{M_k}\sum_{n=1}^{T_k+U_k} t_{k,n} \geqslant 1 \tag{44c}$$
$$\ln\left(M_k P_{2,n}^{(k)} l_{2,n}^{(k,k)}\right)+\ln(1-t_{k,n}) \geqslant \ln(z_k|z_k^{s-1})+\ln(t_{k,n}|t_{k,n}^{s-1})+\ln(\sigma_{k,2}^2(\mathbf{P}|\mathbf{P}^{s-1})) \tag{44d}$$
$$w_{k,m}\geqslant 0, z_k\geqslant 1, t_{k,n}\geqslant 0 \tag{44e}$$
$$\mathbf{P}^{(k)} \succeq 0 \tag{44f}$$
$$\text{tr}(\mathbf{P}^{(k)}) \leqslant P_{\max} \tag{44g}$$

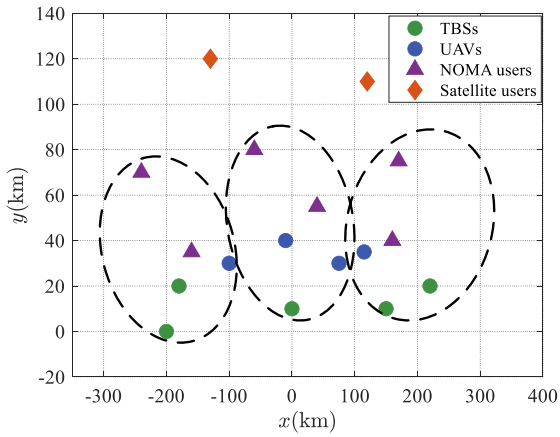

Fig. 2. Illustration of the network topology in simulations.

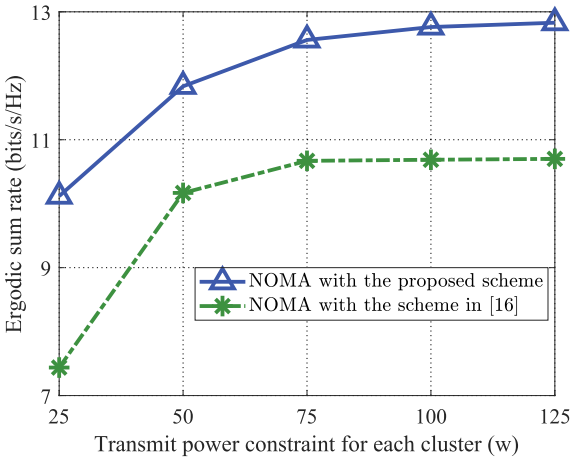

Fig. 3. Ergodic sum rate with different power allocation schemes under the NOMA regime.

$$P_n^{(k)} \leqslant P_{\text{Tmax}}, \quad n=1,\ldots,T_k \tag{44h}$$
$$P_n^{(k)} \leqslant P_{\text{Umax}}, \quad n=T_k+1,\ldots,T_k+U_k \tag{44i}$$
$$\sum_{k=1}^{K}\sum_{n=1}^{T_k+U_k} P_n^{(k)} l'^{(j,k)}_n \leqslant \bar{P}, \quad j=1,\ldots,J \tag{44j}$$
$$m=1,2, \quad n=1,\ldots,T_k+U_k, \quad k=1,\ldots,K,$$

where the expressions $\mathcal{G}(\mathbf{P},\mathbf{w}|\mathbf{P}^{s-1})$, $\mathcal{F}_k(z_k,\mathbf{t}_k|\mathbf{t}_k^{s-1})$ and $\ln(z_k|z_k^{s-1})+\ln(t_{k,n}|t_{k,n}^{s-1})+\ln(\sigma_{k,2}^2(\mathbf{P}|\mathbf{P}^{s-1}))$ as well as $\sigma_{k,1}^2(\mathbf{P}|\mathbf{P}^{s-1})$, $\sigma_{k,2}^2(\mathbf{P}|\mathbf{P}^{s-1})$ are shown at the bottom of the next page. The algorithm is summarized in **Algorithm 1**. Its convergence is shown in the following *Lemma 2*.

Lemma 2: **Algorithm 1** is assured to converge, at least to a local optimum.

Proof: See Appendix C.

IV. Simulation Results and Discussion

In this section, we evaluate the proposed scheme through simulations. Without loss of generality, we assume there are three nearshore clusters, i.e., $K=3$, consisting of $T_1=T_3=2$, $T_2=1$ TBSs and $U_1=U_3=1$, $U_2=2$ UAVs. In each cluster, two NOMA users are located within 100km from the coastline. Both TBSs and UAVs are equipped with

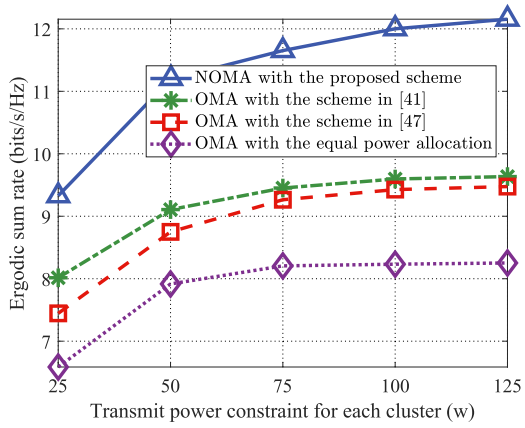

Fig. 4. Ergodic sum rate with different power allocation schemes, under both NOMA and OMA regimes.

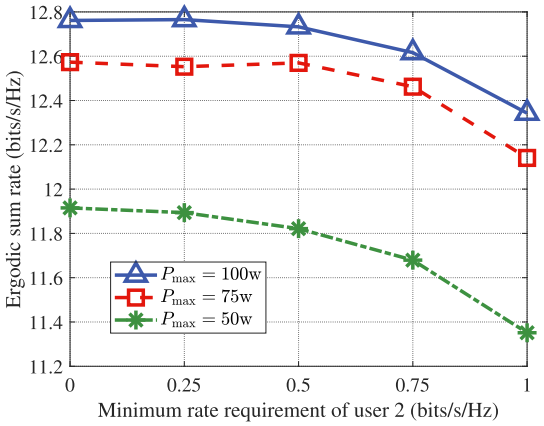

Fig. 5. Ergodic sum rate with different transmit power constraints, varying with the minimum rate requirement of user 2.

a single antenna, and NOMA users are equipped with three antennas, i.e., $M_1 = M_2 = M_3 = 3$. Beyond clusters, there are two satellite users that use the same frequency band as

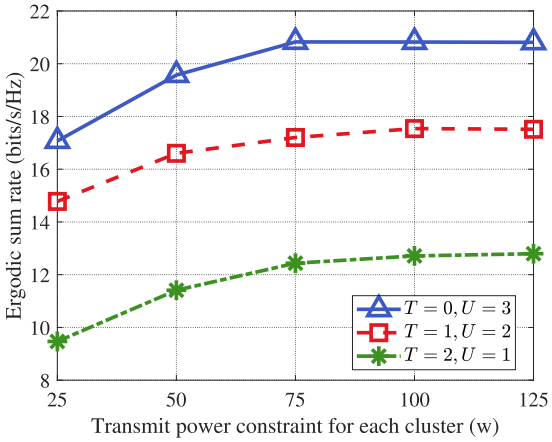

Fig. 6. Ergodic sum rate with different configurations of TBSs and UAVs.

considered NOMA users, i.e., $J = 2$, and their maximum tolerable interference is -100dBm [44]. To provide wide-area coverage, the maximum transmit power of TBSs and UAVs is set as 40w and 30w, i.e., $P_{\text{Tmax}} = 40\text{w}, P_{\text{Umax}} = 30\text{w}$ [35]. In addition, TBSs are high-located at the altitude of 200m [45], UAVs hover at an altitude of 800m and the height of user terminal is 5m, i.e., $h_u = 800\text{m}$, $h_t = 200\text{m}$ and $h_r = 5\text{m}$. Based on the link budget, we further assume the antenna gains of TBSs and UAVs are 23dBi and 3dBi, i.e., $g_t = 23/3\text{dBi}$ [46], and the antenna gain of receivers is 7dBi, i.e., $g_r = 7\text{dBi}$. The minimum rate requirement of user 2 is 0.5 bits/s/Hz, i.e., $r_1 = r_2 = r_3 = 0.5$ bits/s/Hz. The maximum transmit power of each cluster changes from 25w to 125w. Channel related parameters are given by $c = 3 \times 10^8$m/s, $\sigma^2 = -107$dBm, $f_c = 2$GHz, $a = 5.0188$, $b = 0.3511$, $\eta_{LOS} = 0.1$, $\eta_{NLOS} = 21$, and $C = 1$.

$$\sigma_{k,1}^2(\mathbf{P}|\mathbf{P}^{s-1}) = \sum_{i=1,i\neq k}^{K} \sum_{n=1}^{T_i+U_i} l_{1,n}^{(k,i)} \left(P_n^{(i)} - (P_n^{(i)})^{s-1}\right) + \sigma^2 \tag{45a}$$

$$\sigma_{k,2}^2(\mathbf{P}|\mathbf{P}^{s-1}) = \sum_{i=1,i\neq k}^{K} \sum_{n=1}^{T_i+U_i} l_{2,n}^{(k,i)} \left(P_n^{(i)} - (P_n^{(i)})^{s-1}\right) + \sum_{n=1}^{T_k+U_k} l_{2,n}^{(k,k)} \left(P_{1,n}^{(k)} - (P_{1,n}^{(k)})^{s-1}\right) + \sigma^2 \tag{45b}$$

$$\mathcal{G}(\mathbf{P}, \mathbf{w}|\mathbf{P}^{s-1}) = \sum_{k=1}^{K} \sum_{m=1}^{2} \mathcal{G}_{k,m}(\mathbf{P}, w_{k,m}|\mathbf{P}^{s-1}) \tag{46a}$$

$$\begin{aligned}\mathcal{G}_{k,m}(\mathbf{P}, w_{k,m}|\mathbf{P}^{s-1}) &= \mathcal{G}_{k,m,1}(\mathbf{P}, w_{k,m}) - \mathcal{G}_{k,m,2}(\mathbf{P}|\mathbf{P}^{s-1}) \\ &= \mathcal{G}_{k,m,1}(\mathbf{P}, w_{k,m}) - \mathcal{G}_{k,m,2}(\mathbf{P}^{s-1}) - (T_k + U_k)\log_2(e)\frac{\sigma_{k,m}^2(\mathbf{P}|\mathbf{P}^{s-1})}{\sigma_{k,m}^2(\mathbf{P}^{s-1})}\end{aligned} \tag{46b}$$

$$\mathcal{F}_k(z_k, \mathbf{t}_k|\mathbf{t}_k^{s-1}) = M_k \log_2 z_k + \sum_{n=1}^{T_k+U_k} \left(\log_2(e)\frac{t_{k,n}^{s-1}(t_{k,n}-1)}{1-t_{k,n}^{s-1}} - \log_2(1-t_{k,n}^{s-1})\right) \tag{47}$$

$$\ln\left(z_k|z_k^{s-1}\right) + \ln\left(t_{k,n}|t_{k,n}^{s-1}\right) + \ln\left(\sigma_{k,2}^2(\mathbf{P}|\mathbf{P}^{s-1})\right) = \ln\left(z_k^{s-1}t_{k,n}^{s-1}\sigma_{k,2}^2(\mathbf{P}^{s-1})\right) + \frac{z_k}{z_k^{s-1}} + \frac{t_{k,n}}{t_{k,n}^{s-1}} + \frac{\sigma_{k,2}^2(\mathbf{P}|\mathbf{P}^{s-1})}{\sigma_{k,2}^2(\mathbf{P}^{s-1})} - 2 \tag{48}$$

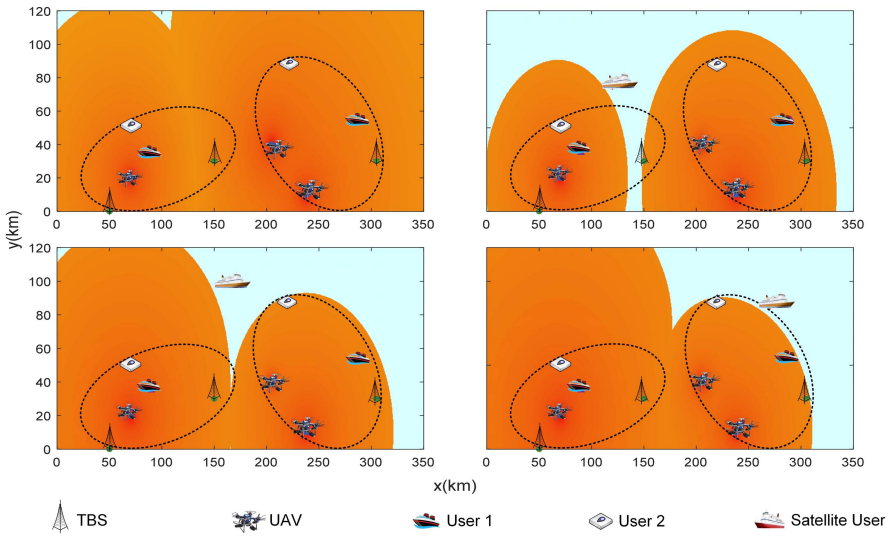

Fig. 7. Illustration of the coverage patterns of nearshore clusters, varying with satellite user locations.

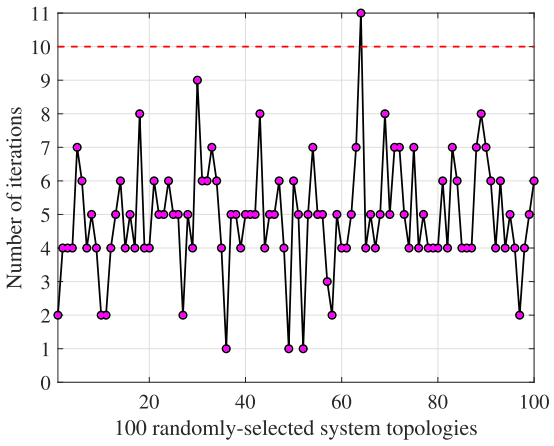

Fig. 8. Convergence performance of the proposed iterative algorithm.

To ensure the NOMA scheme is applicable, we choose a topology where user 1 and user 2 are far apart so that the condition (16) is guaranteed. The specific distribution is shown in Fig. 2, and the positive direction of y points to the sea.

First, we evaluate the proposed scheme and compare it with the scheme in [16]. As we can see from Fig. 3, the proposed scheme achieves much higher rate than that of [16]. We can also find that when the maximum transmit power exceeds 75w, increasing power cannot increase the sum rate under the scheme in [16]. This means the system is saturated due to severe interference. For the proposed scheme, the saturated point does not yet occur in this figure. It can be explained that, based on the large-scale CSI, the system could smartly allocate the power to balance its positive effects of useful signals for its own cluster and the negative impact of harmful interference for other clusters.

Second, we compare the proposed scheme based on NOMA with three OMA schemes proposed in [41] and [47] as well as the scheme of equal power allocation. Without loss of generality, the allocation coefficient of OMA users is set as $\frac{1}{2}$, and we use the averaged ergodic rate of user 2 under the OMA scheme proposed in [41] as the minimal user rate for the proposed scheme. As shown in Fig. 4, the proposed NOMA scheme remarkably outperforms the other three OMA schemes. These gains are achieved at the cost of more complex receivers. The inter-user interference is reduced by SIC. In addition, since NOMA separates users in the power domain, it provides additional flexibility to optimize the power allocation between paired users. But for OMA, it is difficult to achieve flexible time or frequency partitioning so that the resource efficiency is not fully exploited. In addition, one can also find that the scheme proposed in [41] performs better than the other two OMA schemes. This can be explained by the fact that, in [41] the interference is effectively controlled based on the large-scale CSI. This further shows that large-scale CSI is effective in mitigating complex interference for irregular settings.

Next, we evaluate the impact of different rate requirements of user 2. As we can see from Fig. 5, the system experiences very small performance degradation as the rate requirement increases, only less than 6% in our settings. This shows that NOMA is capable of supporting the wide sparsity of maritime IoT, satisfying the basic QoS requirement of user 2 without sacrificing much system efficiency to provide high-rate connections for user 1. From another perspective, the increasing downward trend of the curve implies that the system efficiency would be largely impacted when there is a high-rate far user. In this case, it may be a better choice to use a resource block to serve the user only but not share with others.

In Fig. 6, we show the superiority of UAVs for coverage enhancement. Different from the above settings, in this simulation, we keep the topology unchanged and replace the original TBSs with UAVs or vice versa. We set $T_1 = T_2 = T_3 = T$, $U_1 = U_2 = U_3 = U$. Clearly, UAVs bring considerable system gains compared with TBSs, with more than 50% rate improvement of one more UAV and one less TBS. This is mainly because of the UAVs' height merit which helps build

high-quality LOS links. Besides, we want to note that the case of TBSs only is not presented for the fact that TBSs only cannot support the basic need of user 2. This indicates that with the assistance of UAVs, the coverage scope of the nearshore network is enlarged.

The impact of inter-segment interference is shown in Fig. 7. In this simulation, we consider the spectrum sharing among two clusters and one satellite user. Orange areas denote the coverage region of nearshore clusters and the left-top subfigure provides the benchmark case of no satellite user. The coverage scope is determined by the received SINR, whose threshold is set to be -5dB and the maximal tolerable interference of the satellite user is set to be -105dBm, i.e., $\bar{P} = -105$dBm. It is obvious that the coverage scope shrinks considerably when there exists a satellite user in nearshore areas, and the coverage pattern changes with satellite user locations. This is attributed to the adaptive power allocation of nearshore clusters. Once the inter-segment interference exceeds the given threshold, the power of BSs near the satellite user is reduced and reallocated to far BSs. Sometimes, some BSs are even muted to control the radiating power. As shown in the right-above subfigure, the coverage region of two clusters is split into two isolated parts. The reason is that the TBS locates at (150km, 30km) is muted since it is the main source for both inter-cluster and inter-segment interference.

Finally, the algorithm convergence is shown in Fig. 8. We randomly generate 100 different typologies with $P_{\max} = 50$w. In most cases, the proposed iterative algorithm only takes less than 10 times to converge, which shows great potential to achieve timely resource allocation in reality.

V. Conclusion

In this paper, we have investigated a NOMA-based hybrid satellite-UAV-terrestrial network on the sea. Particularly, we have utilized tethered UAVs to coordinate with TBSs. They form virtual clusters and serve users in a user-centric manner. To accommodate the wide sparsity of the maritime IoT, the NOMA technique has been applied to agilely serve different users. The spectrum sharing has been considered between nearshore clusters and marine satellites. We have proposed a joint power allocation scheme to tackle the challenging interference among different users, different clusters, and different network segments. Based on large-scale CSI only, the ergodic sum rate has been maximized at a low cost. To tackle the non-convex problem, we have transformed our problem into a max-min problem and applied auxiliary functions to simplify the troubling non-linear constraints. An iterative algorithm has been proposed to find the solution by solving a series of optimization-friendly subproblems. Simulation results have shown the potential of NOMA-based hybrid satellite-UAV-terrestrial networks for the maritime coverage enhancement.

Appendix A
Proof of *Theorem 1*

Through observations, (27c) can be rewritten as

$$1-(v_{k,2}^*)^{-1} = \sum_{n=1}^{T_k+U_k} \frac{l_{2,n}^{(k,k)} P_{2,n}^{(k)}}{v_{k,2}^* \sigma_{k,2}^2(\mathbf{P}) + M_k l_{2,n}^{(k,k)} P_{2,n}^{(k)}}. \quad (49)$$

Based on this transformation, the term $1-(v_{k,2}^*)^{-1}$ in $g_{k,2}(\mathbf{P}, v_{k,2}^*)$ (defined in (23b)) can be replaced by the right side of (49). Consequently, we construct the auxiliary function $f_k(\mathbf{P}, z_k)$,

$$\begin{aligned} f_k(\mathbf{P}, z_k) = \sum_{n=1}^{T_k+U_k} \Bigg(& \log_2\left(1+\frac{M_k l_{2,n}^{(k,k)} P_{2,n}^{(k)}}{z_k \sigma_{k,2}^2(\mathbf{P})}\right) \\ & - \frac{\log_2(e) M_k l_{2,n}^{(k,k)} P_{2,n}^{(k)}}{z_k \sigma_{k,2}^2(\mathbf{P}) + M_k l_{2,n}^{(k,k)} P_{2,n}^{(k)}} \Bigg) \\ & + M_k \log_2 z_k, \end{aligned} \quad (50)$$

where z_k is the introduced variable corresponding to $v_{2,k}^*$. Based on the equality (49), we have

$$g_{k,2}(\mathbf{P}, v_{2,k}^*) = f_k(\mathbf{P}, v_{2,k}^*). \quad (51)$$

Next, we prove the increasing monotonicity of $f_k(\mathbf{P}, z_k)$ with respect to z_k. We calculate the partial derivative of $f_k(\mathbf{P}, z_k)$,

$$\begin{aligned} & \frac{\partial f_k(\mathbf{P}, z_k)}{\partial z_k} \\ & = \frac{\log_2 e}{z_k}\left[M_k - \sum_{n=1}^{T_k+U_k} \left(\frac{M_k l_{2,n}^{(k,k)} P_{2,n}^{(k)}}{z_k \sigma_{k,2}^2(\mathbf{P}) + M_k l_{2,n}^{(k,k)} P_{2,n}^{(k)}}\right)^2\right] \\ & > \frac{\log_2 e}{z_k}[M_k - (T_k+U_k)]. \end{aligned} \quad (52)$$

When $M_k \geqslant T_k + U_k$, the partial derivative is positive and $f_k(\mathbf{P}, z_k)$ monotonically increases with z_k. Based on the monotonicity of $f_k(\mathbf{P}, z_k)$ and equation (51), we could draw the following equation,

$$g_{k,2}(\mathbf{P}, v_{k,2}^*) = \max_{1 \leqslant z_k \leqslant v_{k,2}^*} f_k(\mathbf{P}, z_k), \quad (53)$$

and *Theorem 1* is proved.

Appendix B
Proof of *Lemma 1*

We prove this by the method of reduction to absurdity. First, if $\{\hat{\mathbf{P}}, \hat{z}_k, \hat{\mathbf{t}}_k, \hat{\mathbf{v}}\}$ is an optimal solution to (P5), and thus $\hat{\mathbf{P}}$ is also the optimal solution to (P2). Assuming $\hat{\mathbf{P}}$ is not the optimal solution to (P2), we could find another solution, defined as $\tilde{\mathbf{P}}$, which is optimal to (P2) and this indicates

$$g(\tilde{\mathbf{P}}, \tilde{\mathbf{v}}) > g(\hat{\mathbf{P}}, \hat{\mathbf{v}}), \quad (54)$$

where $\hat{\mathbf{v}}$ and $\tilde{\mathbf{v}}$ are determined by the non-linear equation of (25c). Based on $\tilde{\mathbf{P}}$ and $\tilde{\mathbf{v}}$, we define $\tilde{z}_k$ and $\tilde{\mathbf{t}}_k = \{\tilde{t}_{k,n} | n = 1, \ldots, T_k + U_k\}, k = 1, \ldots, K$ as follows

$$\tilde{z}_k = \tilde{v}_{k,2}, \quad (55a)$$

$$\tilde{t}_{k,n} = \frac{M_k l_{2,n}^{(k,k)} \tilde{P}_{2,n}^{(k)}}{\tilde{z}_k \sigma_{k,2}^2(\tilde{\mathbf{P}}) + M_k l_{2,n}^{(k,k)} \tilde{P}_{2,n}^{(k)}}. \quad (55b)$$

Referring to (29), (34) and (35), there exist following equations

$$g_{k,2}(\tilde{\mathbf{P}}, \tilde{v}_{k,2}) = f_k(\tilde{\mathbf{P}}, \tilde{v}_{k,2}) = f_k(\tilde{\mathbf{P}}, \tilde{z}_k) = \mathcal{F}_k(\tilde{z}_k, \tilde{\mathbf{t}}_k). \quad (56)$$

Since $\tilde{\mathbf{P}}$ is optimal to (P2), it meets the constraint (25b), so, we could deduce that

$$g_{k,2}(\tilde{\mathbf{P}}, \tilde{v}_{k,2}) \geqslant r_k \Rightarrow \mathcal{F}(\tilde{z}_k, \tilde{\mathbf{t}}_k) \geqslant r. \quad (57)$$

As shown in (55a), (55b) and (57), we could find $\{\tilde{\mathbf{P}}, \tilde{z}_k, \tilde{\mathbf{t}}_k, \tilde{\mathbf{v}}\}$ is feasible to (P5) and we have $g(\tilde{\mathbf{P}}, \tilde{\mathbf{v}}) > g(\hat{\mathbf{P}}, \hat{\mathbf{v}})$, which is equivalent to

$$\min_{\mathbf{v}} g(\tilde{\mathbf{P}}, \mathbf{v}) > \min_{\mathbf{v}} g(\hat{\mathbf{P}}, \mathbf{v}). \tag{58}$$

This has been explained in (26). It is contradictory that $\{\hat{\mathbf{P}}, \hat{z}_k, \hat{\mathbf{t}}_k, \hat{\mathbf{v}}\}$ is the optimal solution to (P5). So the assumption that there exists other optimal solution to (P2) does not hold and $\hat{\mathbf{P}}$ is optimal to (P2).

Similarly, if $\tilde{\mathbf{P}}$ is the optimal solution to (P2), it also holds the optimality in (P5). If not, there exists $\{\hat{\mathbf{P}}, \hat{z}_k, \hat{\mathbf{t}}_k, \hat{\mathbf{v}}\}$ and we have

$$\min_{\mathbf{v}} g(\hat{\mathbf{P}}, \mathbf{v}) > \min_{\mathbf{v}} g(\tilde{\mathbf{P}}, \mathbf{v}), \tag{59a}$$

$$\Rightarrow g(\hat{\mathbf{P}}, \hat{\mathbf{v}}) > g(\tilde{\mathbf{P}}, \tilde{\mathbf{v}}). \tag{59b}$$

Based on $\hat{\mathbf{P}}$, define $\hat{z'}_k$ and $\hat{\mathbf{t}'}_k = \{\hat{t'}_{k,n} | n = 1, \ldots, T_k + U_k,\ k = 1, \ldots, K\}$ as follows

$$\hat{z'}_k = \hat{v}_{k,2}, \tag{60a}$$

$$\hat{t'}_{k,n} = \frac{M_k l_{2,n}^{(k,k)} \hat{P}_{2,n}^{(k)}}{\hat{z'}_k \sigma_{k,2}^2(\hat{\mathbf{P}}) + M_k l_{2,n}^{(k,k)} \hat{P}_{2,n}^{(k)}}. \tag{60b}$$

Referring to (37c) and (37d), it is easy to find that $\hat{z'}_k \geqslant \hat{z}_k$ and $\hat{t'}_{k,n} \geqslant \hat{t}_{k,n}$. Based on the monotonically increasing characteristic of $\mathcal{F}_k(z_k, \mathbf{t}_k)$, we have that

$$\mathcal{F}_k(\hat{z'}_k, \hat{\mathbf{t}'}_k) \geqslant \mathcal{F}_k(\hat{z}_k, \hat{\mathbf{t}}_k). \tag{61}$$

According to (29) and (35), the following equations hold

$$g_{k,2}(\hat{\mathbf{P}}, \hat{v}_{k,2}) = f_k(\hat{\mathbf{P}}, \hat{v}_{k,2}) = f_k(\hat{\mathbf{P}}, \hat{z'}_k) = \mathcal{F}(\hat{z'}_k, \hat{\mathbf{t}'}_k). \tag{62}$$

Since $\mathcal{F}_k(\hat{z}_k, \hat{\mathbf{t}}_k) \geqslant r_k$, it is affirmed that $\mathcal{F}_k(\hat{z'}_k, \hat{\mathbf{t}'}_k) \geqslant r_k$ and thus $g_{k,2}(\hat{\mathbf{P}}, \hat{v}_{k,2}) \geqslant r_k$. Consequently, $\hat{\mathbf{P}}$ is a feasible solution to (P2) and it achieves a higher value than that of $\tilde{\mathbf{P}}$, which is contradictory that $\tilde{\mathbf{P}}$ is the optimal solution to (P2). So, the assumption that there exists other optimal solution to (P5) does not hold. The optimal equivalence between (P2) and (P5) is thus proven.

APPENDIX C
PROOF OF *Lemma 2*

By applying the Taylor expansion, the tangent of the concave function is above its curve and the tangent of the convex function is below its curve. Since $\log_2(1 - t_{k,n})$ (the term in $\mathcal{F}_k(z_k, \mathbf{t}_k)$) and z_k^{-1} are convex with respect to $t_{k,n}$ and z_k, and $\mathrm{In}(z_k) + \mathrm{In}(t_{k,n}) + \mathrm{In}(\sigma_{k,2}^2(\mathbf{P}))$ is concave with respect to $z_k,\ t_{k,n}$ and $\mathbf{P}$, the following inequalities hold

$$\mathcal{F}_k(z_k, \mathbf{t}_k) \geqslant \mathcal{F}_k(z_k, \mathbf{t}_k | \mathbf{t}_k^{s-1}), \tag{63a}$$

$$\frac{1}{z_k} \geqslant -\frac{z_k}{(z_k^{s-1})^2} + \frac{1}{z_k^{s-1}}, \tag{63b}$$

$$\begin{aligned} &\mathrm{In}(z_k) + \mathrm{In}(t_{k,n}) + \mathrm{In}(\sigma_{k,2}^2(\mathbf{P})) \\ &\quad \leqslant \mathrm{In}(z_k | z_k^{s-1}) + \mathrm{In}(t_{k,n} | t_{k,n}^{s-1}) \\ &\qquad + \mathrm{In}(\sigma_{k,2}^2(\mathbf{P} | \mathbf{P}^{s-1})), \end{aligned} \tag{63c}$$

which makes the constraints (44b), (44c) and (44d) in (P7) tighter than the corresponding constraints in (P6). Thereby, in each iteration, the optimal solution $\mathbf{P}^s$ is guaranteed in the feasible set of the original problem.

For the objective, since $\mathcal{G}_{k,m,2}(\mathbf{P})$ is a concave function with respect to $\mathbf{P}$, it holds that

$$\mathcal{G}_{k,m,2}(\mathbf{P} | \mathbf{P}^{s-1}) \geqslant \mathcal{G}_{k,m,2}(\mathbf{P}). \tag{64}$$

Accordingly, the following inequalities can be obtained

$$\begin{aligned} \mathcal{G}_{k,m}(\mathbf{P}, w_{k,m}) &= \mathcal{G}_{k,m,1}(\mathbf{P}, w_{k,m}) - \mathcal{G}_{k,m,2}(\mathbf{P}) \\ &\geqslant \mathcal{G}_{k,m,1}(\mathbf{P}, w_{k,m}) - \mathcal{G}_{k,m,2}(\mathbf{P} | \mathbf{P}^{s-1}) \\ &= \mathcal{G}_{k,m}(\mathbf{P}, w_{k,m} | \mathbf{P}^{s-1}). \end{aligned} \tag{65}$$

Therefore, we have that

$$\mathcal{G}(\mathbf{P}, \mathbf{w}) \geqslant \mathcal{G}(\mathbf{P}, \mathbf{w} | \mathbf{P}^{s-1}). \tag{66}$$

Furthermore, according to the properties of the saddle point, there are following conclusions for $(\mathbf{P}^s, \mathbf{w}^s)$

$$\begin{aligned} &\mathcal{G}(\mathbf{P}^s, \mathbf{w}^s | \mathbf{P}^{s-1}) \geqslant \mathcal{G}(\mathbf{P}, \mathbf{w}^s | \mathbf{P}^{s-1}), \\ &\mathcal{G}(\mathbf{P}^s, \mathbf{w}^s | \mathbf{P}^{s-1}) \leqslant \mathcal{G}(\mathbf{P}^s, \mathbf{w} | \mathbf{P}^{s-1}). \end{aligned} \tag{67}$$

Based on (66) and (67), the relationship of $\mathcal{G}(\mathbf{P}^s, \mathbf{w}^s)$ and $\mathcal{G}(\mathbf{P}^{s-1}, \mathbf{w}^{s-1})$ can be derived as follows

$$\mathcal{G}(\mathbf{P}^s, \mathbf{w}^s) \geqslant \mathcal{G}(\mathbf{P}^s, \mathbf{w}^s | \mathbf{P}^{s-1}) = \max_{\mathbf{P}} \mathcal{G}(\mathbf{P}, \mathbf{w}^s | \mathbf{P}^{s-1}) \tag{68a}$$

$$\geqslant \mathcal{G}(\mathbf{P}^{s-1}, \mathbf{w}^s | \mathbf{P}^{s-1}) = \mathcal{G}(\mathbf{P}^{s-1}, \mathbf{w}^s) \tag{68b}$$

$$\geqslant \min_{\mathbf{w}} \mathcal{G}(\mathbf{P}^{s-1}, \mathbf{w}) = \mathcal{G}(\mathbf{P}^{s-1}, \mathbf{w}^{s-1}). \tag{68c}$$

Based on the monotonically increasing property of the objective function in iterations, and the fact that the ergodic sum rate is up-bounded, the proposed algorithm is assured to converge, at least to a local optimum.

REFERENCES

[1] Z. Ma, M. Xiao, Y. Xiao, Z. Pang, H. V. Poor, and B. Vucetic, "High-reliability and low-latency wireless communication for Internet of Things: Challenges, fundamentals, and enabling technologies," *IEEE Internet Things J.*, vol. 6, no. 5, pp. 7946–7970, Oct. 2019.

[2] T. Wei, W. Feng, Y. Chen, C.-X. Wang, N. Ge, and J. Lu, "Hybrid satellite-terrestrial communication networks for the maritime Internet of Things: Key technologies, opportunities, and challenges," *IEEE Internet Things J.*, vol. 8, no. 11, pp. 8910–8934, Jun. 2021.

[3] L. Qian *et al.*, "Multi-dimensional polarized modulation for land mobile satellite communications," *IEEE Trans. Cogn. Commun. Netw.*, vol. 7, no. 2, pp. 383–397, Jun. 2021.

[4] H. Chen, M. Xiao, and Z. Pang, "Satellite-based computing networks with federated learning," *IEEE Wireless Commun. Mag.*, vol. 29, no. 1, pp. 78–84, Feb. 2022.

[5] T. Wei, W. Feng, J. Wang, N. Ge, and J. Lu, "Exploiting the shipping lane information for energy-efficient maritime communications," *IEEE Trans. Veh. Technol.*, vol. 68, no. 7, pp. 7204–7208, Jul. 2019.

[6] M. M. Wang, J. Zhang, and X. You, "Machine-type communication for $maritime$ Internet of Things: A design," *IEEE Commun. Surveys Tuts.*, vol. 22, no. 4, pp. 2550–2585, 4th Quart., 2020.

[7] X. Li, W. Feng, J. Wang, Y. Chen, N. Ge, and C.-X. Wang, "Enabling 5G on the ocean: A hybrid satellite-UAV-terrestrial network solution," *IEEE Wireless Commun.*, vol. 27, no. 6, pp. 116–121, Dec. 2020.

[8] M. Mozaffari, W. Saad, M. Bennis, Y.-H. Nam, and M. Debbah, "A tutorial on UAVs for wireless networks: Applications, challenges, and open problems," *IEEE Commun. Surveys Tuts.*, vol. 21, no. 3, pp. 2334–2360, 3rd Quart., 2019.

[9] Y. Zeng, Q. Wu, and R. Zhang, "Accessing from the sky: A tutorial on UAV communications for 5G and beyond," *Proc. IEEE*, vol. 107, no. 12, pp. 2327–2375, Dec. 2019.
[10] C. Zhao, J. Liu, M. Sheng, W. Teng, Y. Zheng, and J. Li, "Multi-UAV trajectory planning for energy-efficient content coverage: A decentralized learning-based approach," *IEEE J. Sel. Areas Commun.*, vol. 39, no. 10, pp. 3193–3207, Oct. 2021.
[11] Z. Xie, J. Liu, M. Sheng, N. Zhao, and J. Li, "Exploiting aerial computing for air-to-ground coverage enhancement," *IEEE Wireless Commun.*, vol. 28, no. 5, pp. 50–58, Oct. 2021.
[12] Y. Li, L. Su, T. Wei, Z. Zhou, and N. Ge, "Location-aware dynamic beam scheduling for maritime communication systems," in *Proc. 10th Int. Conf. Commun., Circuits Syst. (ICCCAS)*, Chengdu, China, Dec. 2018, pp. 265–268.
[13] M. Xu, F. Ji, M. Wen, and W. Duan, "Novel receiver design for the cooperative relaying system with non-orthogonal multiple access," *IEEE Commun. Lett.*, vol. 20, no. 8, pp. 1679–1682, Aug. 2016.
[14] B. Zheng *et al.*, "Secure NOMA based two-way relay networks using artificial noise and full duplex," *IEEE J. Sel. Areas Commun.*, vol. 36, no. 7, pp. 1426–1440, Jul. 2018.
[15] D. Wan, M. Wen, F. Ji, H. Yu, and F. Chen, "Non-orthogonal multiple access for cooperative communications: Challenges, opportunities, and trends," *IEEE Wireless Commun.*, vol. 25, no. 2, pp. 109–117, Apr. 2018.
[16] Q. Sun, S. Han, I. Chin-Lin, and Z. Pan, "On the ergodic capacity of MIMO NOMA systems," *IEEE Wireless Commun. Lett.*, vol. 4, no. 4, pp. 405–408, Aug. 2015.
[17] Z. Ding, F. Adachi, and H. V. Poor, "The application of MIMO to non-orthogonal multiple access," *IEEE Trans. Wireless Commun.*, vol. 15, no. 1, pp. 537–552, Jan. 2016.
[18] X. Li, W. Feng, Y. Chen, C.-X. Wang, and N. Ge, "Maritime coverage enhancement using UAVs coordinated with hybrid satellite-terrestrial networks," *IEEE Trans. Commun.*, vol. 68, no. 4, pp. 2355–2369, Apr. 2020.
[19] X. Fang, Y. Wang, W. Feng, Y. Chen, and B. Ai, "Power allocation for maritime cognitive satellite-UAV-terrestrial networks," in *Proc. IEEE 19th Int. Conf Cogn. Inf., Cogn. Comput. (ICCI*CC)*, Sep. 2020, pp. 139–143.
[20] Y. Wang, X. Fang, W. Feng, Y. Chen, N. Ge, and Z. Lu, "On-demand coverage for maritime hybrid satellite-UAV-terrestrial networks," in *Proc. Int. Conf. Wireless Commun. Signal Process. (WCSP)*, Nanjing, China, Oct. 2020, pp. 483–488.
[21] J. Zhang, F. Liang, B. Li, Z. Yang, Y. Wu, and H. Zhu, "Placement optimization of caching UAV-assisted mobile relay maritime communication," *China Commun.*, vol. 17, no. 8, pp. 209–219, Aug. 2020.
[22] A. Xiao, N. Ge, L. Yin, and C. Jiang, "A voyage-based cooperative resource allocation scheme in maritime broadband access network," in *Proc. IEEE 86th Veh. Technol. Conf. (VTC-Fall)*, Toronto, ON, Canada, Sep. 2017, pp. 1–5.
[23] M. S. Ali, H. Tabassum, and E. Hossain, "Dynamic user clustering and power allocation for uplink and downlink non-orthogonal multiple access (NOMA) systems," *IEEE Access*, vol. 4, pp. 6325–6343, 2016.
[24] Y. Sun, D. W. K. Ng, Z. Ding, and R. Schober, "Optimal joint power and subcarrier allocation for full-duplex multicarrier non-orthogonal multiple access systems," *IEEE Trans. Commun.*, vol. 65, no. 3, pp. 1077–1091, Mar. 2017.
[25] Y. Wu *et al.*, "Optimal power allocation and scheduling for non-orthogonal multiple access relay-assisted networks," *IEEE Trans. Mobile Comput.*, vol. 17, no. 11, pp. 2591–2606, Nov. 2018.
[26] L. Zhang, J. Liu, M. Xiao, G. Wu, Y.-C. Liang, and S. Li, "Performance analysis and optimization in downlink NOMA systems with cooperative full-duplex relaying," *IEEE J. Sel. Areas Commun.*, vol. 35, no. 10, pp. 2398–2412, Oct. 2017.
[27] Q. Sun, S. Han, Z. Xu, S. Wang, I. Chih-Lin, and Z. Pan, "Sum rate optimization for MIMO non-orthogonal multiple access systems," in *Proc. IEEE Wireless Commun. Netw. Conf. (WCNC)*, Mar. 2015, pp. 747–752.
[28] S. Ali, E. Hossain, and D. I. Kim, "Non-orthogonal multiple access (NOMA) for downlink multiuser MIMO systems: User clustering, beamforming, and power allocation," *IEEE Access*, vol. 5, pp. 565–577, 2017.
[29] X. Sun *et al.*, "Joint beamforming and power allocation in downlink NOMA multiuser MIMO networks," *IEEE Trans. Wireless Commun.*, vol. 17, no. 8, pp. 5367–5381, Aug. 2018.
[30] C. Liu, W. Feng, Y. Chen, C.-X. Wang, and N. Ge, "Cell-free satellite-UAV networks for 6G wide-area Internet of Things," *IEEE J. Sel. Areas Commun.*, vol. 39, no. 4, pp. 1116–1131, Apr. 2021.
[31] X. Zhu, C. Jiang, L. Kuang, N. Ge, and J. Lu, "Non-orthogonal multiple access based integrated terrestrial-satellite networks," *IEEE J. Sel. Areas Commun.*, vol. 35, no. 10, pp. 2253–2267, Oct. 2017.
[32] Z. Lin, M. Lin, J.-B. Wang, T. de Cola, and J. Wang, "Joint beamforming and power allocation for satellite-terrestrial integrated networks with non-orthogonal multiple access," *IEEE J. Sel. Areas Commun.*, vol. 13, no. 3, pp. 657–670, Jun. 2019.
[33] N. Zhao *et al.*, "Joint trajectory and precoding optimization for UAV-assisted NOMA networks," *IEEE Trans. Commun.*, vol. 67, no. 5, pp. 3723–3735, May 2019.
[34] X. Pang *et al.*, "UAV-aided NOMA networks with optimization of trajectory and precoding," in *Proc. 10th Int. Conf. Wireless Commun. Signal Process. (WCSP)*, Oct. 2018, pp. 1–6.
[35] S. Jo and W. Shim, "LTE-maritime: High-speed maritime wireless communication based on LTE technology," *IEEE Access*, vol. 7, pp. 53172–53181, 2019.
[36] A. Al-Hourani, S. Kandeepan, and S. Lardner, "Optimal LAP altitude for maximum coverage," *IEEE Wireless Commun. Lett.*, vol. 3, no. 6, pp. 569–572, Dec. 2014.
[37] P. Wang, W. Zhang, J. Yin, L. Li, H. Xie, and S. Ma, "AIS data-based for statistics and analysis of maritime traffic dangerous features: A case study of San Diego costal water," in *Proc. Chin. Control Decis. Conf. (CCDC)*, Hefei, China, 2020, pp. 3671–3676.
[38] W. Choi and J. G. Andrews, "The capacity gain from intercell scheduling in multi-antenna systems," *IEEE Trans. Wireless Commun.*, vol. 7, no. 2, pp. 714–725, Feb. 2008.
[39] Z. Ding *et al.*, "Impact of user pairing on 5G nonorthogonal multiple-access downlink transmissions," *IEEE Trans. Veh. Technol.*, vol. 65, no. 8, pp. 6010–6023, Aug. 2016.
[40] Y. Wang and Z. Lu, "Coordinated resource allocation for satellite-terrestrial coexistence based on radio maps," *China Commun.*, vol. 15, no. 3, pp. 149–156, Mar. 2018.
[41] W. Feng, Y. Wang, N. Ge, J. Lu, and J. Zhang, "Virtual MIMO in multi-cell distributed antenna systems: Coordinated transmissions with large-scale CSIT," *IEEE J. Sel. Areas Commun.*, vol. 31, no. 10, pp. 2067–2081, Oct. 2013.
[42] A. M. Tulino and S. Verdú, "Random matrix theory and wireless communications," *Found. Trends Commun. Inf. Theory*, vol. 1, no. 1, pp. 1–182, 2004.
[43] W. Feng, Y. Li, S. Zhou, J. Wang, and M. Xia, "Downlink capacity of distributed antenna systems in a multi-cell environment," in *Proc. IEEE Wireless Commun. Netw. Conf.*, Apr. 2009, pp. 1–5.
[44] W. Feng, N. Ge, and J. Lu, "Coordinated satellite-terrestrial networks: A robust spectrum sharing perspective," in *Proc. 26th Wireless Opt. Commun. Conf. (WOCC)*, 2017, pp. 1–5.
[45] H. Seo, J. Shim, S. Ha, Y. S. Kim, and J. Jeong, "Ultra long range LTE ocean coverage solution," in *Proc. 24th Int. Conf. Telecommun. (ICT)*, 2017, pp. 1–5.
[46] Y. Zhao, J. Ren, and X. Chi, "Maritime mobile channel transmission model based on ITM," in *Proc. 2nd Int. Symp. Comput., Commun., Control Autom.* Amsterdam, The Netherlands: Atlantis Press, 2013.
[47] W. Choi and J. G. Andrews, "Downlink performance and capacity of distributed antenna systems in a multicell environment," *IEEE Trans. Wireless Commun.*, vol. 6, no. 1, pp. 69–73, Jan. 2007.

Xinran Fang (Student Member, IEEE) received the B.S. degree from the School of Electronic and Information Engineering, Beijing Jiaotong University, Beijing, China, in 2020. She is currently pursuing the Ph.D. degree with the Department of Electronic Engineering, Tsinghua University, Beijing. Her research interests include maritime communication, hybrid satellite–UAV-terrestrial networks, UAV communication, and joint communication and sensing.

Wei Feng (Senior Member, IEEE) received the B.S. and Ph.D. degrees from the Department of Electronic Engineering, Tsinghua University, Beijing, China, in 2005 and 2010, respectively. He is currently a Professor with the Department of Electronic Engineering, Tsinghua University. His research interests include maritime communication networks, large-scale distributed antenna systems, and coordinated satellite-UAV-terrestrial networks. He serves as the Assistant to the Editor-in-Chief for *China Communications* and an Editor for IEEE TRANSACTIONS ON COGNITIVE COMMUNICATIONS AND NETWORKING.

Yanmin Wang received the B.S. degree from Shandong University, China, in 2008, and the Ph.D. degree from the Department of Electronic Engineering, Tsinghua University, Beijing, China, in 2013. She is currently an Associate Professor at the School of Information Engineering, Minzu University of China. Her research interests include distributed antenna systems, satellite networks, and coordinated satellite-UAV-terrestrial networks.

Yunfei Chen (Senior Member, IEEE) received the B.E. and M.E. degrees in electronics engineering from Shanghai Jiao Tong University, Shanghai, China, in 1998 and 2001, respectively, and the Ph.D. degree from the University of Alberta, Edmonton, AB, Canada, in 2006.

He is currently working as a Reader of the School of Engineering, University of Warwick, Coventry, U.K. His research interests include wireless communications, performance analysis, joint radar-communications designs, cognitive radios, wireless relaying, and energy harvesting.

Ning Ge (Member, IEEE) received the B.S. and Ph.D. degrees from Tsinghua University, Beijing, China, in 1993 and 1997, respectively. From 1998 to 2000, he worked on the development of ATM switch fabric ASIC at ADC Telecommunications, Dallas. Since 2000, he has been with the Department of Electronics Engineering, Tsinghua University, where he is currently a Professor. His research interests include ASIC design, short-range wireless communication, and satellite communications. He is a Senior Member of CIC and CIE.

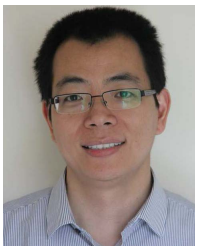

Zhiguo Ding (Fellow, IEEE) received the B.Eng. degree in electrical engineering from the Beijing University of Posts and Telecommunications in 2000 and the Ph.D. degree in electrical engineering from Imperial College London in 2005.

From July 2005 to April 2018, he was working at Queen's University Belfast, Imperial College, Newcastle University, and Lancaster University. From October 2012 to September 2022, he was an Academic Visitor at Princeton University. Since April 2018, he has been with The University of Manchester as a Professor in communications. His research interests are B5G networks, machine learning, cooperative and energy harvesting networks, and statistical signal processing. He is a Distinguished Lecturer of IEEE ComSoc and a Web of Science Highly Cited Researcher in two categories 2020. He recently received the EU Marie Curie Fellowship 2012–2014, the Top IEEE TRANSACTIONS ON VEHICULAR TECHNOLOGY Editor in 2017, the IEEE Heinrich Hertz Award in 2018, the IEEE Jack Neubauer Memorial Award in 2018, the IEEE Best Signal Processing Letter Award in 2018, the Friedrich Wilhelm Bessel Research Award in 2020, and the Best Paper Award at IEEE ICCC-2021. He is serving as an Area Editor for the IEEE OPEN JOURNAL OF THE COMMUNICATIONS SOCIETY, an Editor for IEEE TRANSACTIONS ON VEHICULAR TECHNOLOGY and IEEE COMMUNICATIONS SURVEYS & TUTORIALS, and was an Editor for IEEE WIRELESS COMMUNICATION LETTERS, IEEE TRANSACTIONS ON COMMUNICATIONS, and IEEE COMMUNICATION LETTERS, from 2013 to 2016.

Hongbo Zhu received the B.S. degree in communications engineering from the Nanjing University of Posts and Telecommunications, Nanjing, China, in 1982, and the Ph.D. degree in information and communications engineering from the Beijing University of Posts and Telecommunications, Beijing, China, in 1996. He is currently a Professor with the Nanjing University of Posts and Telecommunications. He is also the Head of the Coordination Innovative Center of IoT Technology and Application (Jiangsu), which is the first government authorized Coordination Innovative Center of IoT in China. He also serves as a referee or expert in multiple national organizations and committees. He has authored or coauthored over 200 technical papers published in various journals and conferences. He is currently leading a big group and multiple funds on the IoT and wireless communications with current focus on architecture and enabling technologies for the Internet of Things. His research interests include mobile communications, wireless communication theory, and electromagnetic compatibility.